Cancer Letters 597 (2024) 217064

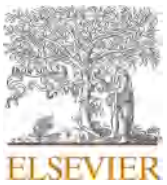

Contents lists available at ScienceDirect

Cancer Letters

journal homepage: www.elsevier.com/locate/canlet

Original Articles

YBX1 promotes homologous recombination and resistance to platinum-induced stress in ovarian cancer by recognizing m5C modification

Huangyang Meng [a,b,c,1], Huixian Miao [a,b,c,1], Yashuang Zhang [a,b,c,1], Tian Chen [a,b,1], Lin Yuan [a,b], Yicong Wan [a,b], Yi Jiang [a,b], Lin Zhang [a,b,c,**], Wenjun Cheng [a,b,c,*]

[a] Department of Gynecology, the First Affiliated Hospital of Nanjing Medical University, Nanjing, 210029, Jiangsu, China
[b] Branch Of National Clinical Research Center For Gynecology and Obstetrics, China
[c] Maternal and Child Center Laboratory, The First Affiliated Hospital of Nanjing Medical University, Nanjing, China

ARTICLE INFO

Keywords:
YBX1
m5C
Ovarian cancer
Homologous recombination
Chemoresistance

ABSTRACT

Platinum-based chemotherapy causes genetic damage and induces apoptosis in ovarian cancer cells. Enhancing the ability to resist platinum drug-induced DNA damage and apoptotic stress is critical for tumor cells to acquire drug resistance. Here, we found that Y-box binding protein 1 (YBX1) was highly expressed in cisplatin-resistant patient-derived organoids (PDOs) and was a crucial gene for alleviating platinum-induced stress and maintaining drug resistance characteristics in ovarian cancer cells. Mechanistically, YBX1 recognized m5C modifications in CHD3 mRNA and maintained mRNA stability by recruiting PABPC1 protein. This regulatory process enhanced chromatin accessibility and improved the efficiency of homologous recombination (HR) repair, facilitating tumor cells to withstand platinum-induced apoptotic stress. In addition, SU056, an inhibitor of YBX1, exhibited the potential to reverse platinum resistance in subcutaneous and PDO orthotopic xenograft models. In conclusion, YBX1 is critical for ovarian cancer cells to alleviate the platinum-induced stress and may be a potential target for reversing drug-resistant therapies.

1. Introduction

Ovarian cancer is the most lethal gynecologic malignancy, with a 5-year survival rate of approximately 30–40 % [1]. The standard treatment for ovarian cancer is tumor debulking surgery combined with platinum-based chemotherapy and maintenance with PARP inhibitors or anti-angiogenic drugs [2]. Most patients can achieve complete response; however, these patients will recur within 1–2 years, along with varying degrees of progressive resistance to chemotherapeutic agents, leading to failure of subsequent treatment. Notably, approximately 15 % of patients relapse within 6 months after completion of chemotherapy. These patients are also known as platinum refractory and exert resistance to almost all agents, with a 5-year survival rate of 10 % merely [3,4]. Understanding the molecular mechanisms of the platinum resistance is crucial for the development of effective therapeutic intervention.

Platinum agents can damage the structure and function of DNA after entering cells and cause DNA double-strand breaks (DSBs) [5]. The main repair mechanisms for DSBs include homologous recombination (HR) and non-homologous end joining (NHEJ) [6]. However, prior to the initiation of DSB repair, the chromatin region near the damaged DNA sites needs to be relaxed by helicase, allowing the access of DNA repair-related enzymes to this region to initiate the subsequent repair process, which is also known as chromatin remodeling [7]. Several studies have identified efficient chromatin remodeling to be associated with drug chemoresistance [8–11], but its role in platinum resistance of ovarian cancer has not been elucidated.

Recently, RNA 5-methylcytosine (m5C), an emerging epigenetic modification, has been reported to play an important role in chromatin organization [12], HR [13] and stress response [14]. Methyltransferases (writers), demethylases (erasers), and recognition proteins (readers) constitute an enzyme system for the dynamic regulation of m5C modification [15], which could regulate mRNA export [16], mRNA stability [17] and long-distance transport [18]. Several studies have revealed an

* Corresponding author. Department of Gynecology, the First Affiliated Hospital of Nanjing Medical University, Nanjing, 210029, Jiangsu, China.
** Corresponding author. Department of Gynecology, the First Affiliated Hospital of Nanjing Medical University, Nanjing, 210029, Jiangsu, China.
E-mail addresses: Davidzhang@njmu.edu.cn (L. Zhang), chengwenjun@jsph.org.cn (W. Cheng).
[1] These authors contributed equally.

https://doi.org/10.1016/j.canlet.2024.217064
Received 24 March 2024; Received in revised form 20 May 2024; Accepted 10 June 2024
Available online 14 June 2024
0304-3835/© 2024 The Authors. Published by Elsevier B.V. This is an open access article under the CC BY-NC-ND license (http://creativecommons.org/licenses/by-nc-nd/4.0/).

association between m5C-related genes and chemoresistance. NSUN2 promoted resistance to radio-chemotherapy in an m5C methylation-dependent manner in esophageal squamous carcinoma [19]. Besides, RCMTs mediated chromatin organization and 5-azacytidine resistance in leukemia [12]. Y-box binding protein 1 (YBX1), a member of the cold shock binding protein family, was recently reported as a reader of m5C modifications [17]. Previous studies suggested that YBX1 enhanced tumor drug resistance through promoting multiple drug-resistance gene expression [20,21]. It motivated us to consider whether the YBX1 protein might involve in the regulation of platinum drug resistance through the m5C epigenetic regulatory mechanism. In the present study, we found that YBX1 could respond to platinum-induced cellular stress. Mechanistically, YBX1 recruited PABPC1 protein by recognizing the m5C modification in CHD3 mRNA to maintain mRNA stability and protein expression. Chromatin remodeling and HR repair capacity were therefore promoted. YBX1 might be a novel target for reversing platinum resistance.

2. Material and methods

2.1. Patient samples

The 20 patient-derived organoids (PDOs), 66 cases of platinum-resistant ovarian cancer tissue, and 229 cases of platinum-sensitive ovarian tissue were all obtained from newly diagnosed OC patients who underwent gynecological surgeries at the First Affiliated Hospital of Nanjing Medical University. All the pathological diagnosis were confirmed by experienced pathologists. The signed informed consent forms were obtained, and the use of clinical samples in this study was approved by the Ethics Committee of the First Affiliated Hospital of Nanjing Medical University (Approval number: 2020-MD-061.A1). Comprehensive clinical and pathological information about ovarian cancer patients can be found in Table S1.

2.2. Organoid construction and passage

The methodology for creating PDOs was based on the protocol reported by Oded Kopper [22]. Fresh tissues obtained from the operating room were promptly transferred to a highly sterile workbench for organoids construction. The tissues were thoroughly washed with pre-cooled PBS buffer. Scissors and forceps were used to remove any bloodstains or necrotic areas from the tissue surface. The tissues were then divided into pieces of 2 × 3 mm and centrifuged. The precipitation was resuspended in the digestion solution consisting of collagenase (SCR103, Sigma, MA), and dispase (D-4693, Sigma, MA), and incubated in a 37-degree water bath until the tissues were broken down into 10–20 cell clusters. Any sizable clumps of tissue not wholly digested were sieved out using a 70 μm filter, and suitable cell clusters were transferred to a 15 mL centrifuge tube. After centrifugation, the pellet was resuspended in a matrix gel, and inoculated into a 48-well plate. The plate was then placed in a cell incubator for 20 min to solidify the matrix gel, after which 200 μL growth medium was added to each well. The organoids were refreshed with fresh culture medium every 3 days and passaged every 2–3 weeks.

2.3. Organoid viability

After digestion, organoids were planted in a 96-well plate at a density of 2000 cells per well. 100 μL of organoid culture medium was added to each well, followed by respective treatments for experimental purposes. Different concentrations (1, 20, 40, 60, 80, 100 μmol/L) of cisplatin were added to the organoid culture medium. After 48 h, the treated organoids were then digested from the 96-well plate and transferred to a 1.5 mL EP tube by centrifuging at 1000 rpm for 10 min. Supernatants were removed, and 100 μL of CellTiter-Lumi luminescence solution was added. The IC50 was calculated based on the data obtained using a multifunctional enzyme-linked immunosorbent assay with a detection time of 0.25–1 s per well. Finally, the organoids were stained using cyto3D Live-Dead Assay kit (BM01, Well bioscience, NJ). Live cells and dead cells were marked with green and red, respectively. Images were captured using a fluorescence microscope.

2.4. Cell culture

The HO8910 cells were procured from the National Cell Line Resource Infrastructure Center in Beijing. The cells were cultured in RPMI 1640 medium with 10 % fetal bovine serum (FBS), penicillin (100 U/ml) and streptomycin (200 μg/ml) provided by GIBCO. The cells were maintained at a temperature of 37 °C in a 5 % carbon dioxide incubator.

2.5. Plasmid transfection and lentivirus infection

For transient transfection, Lipofectamine 3000 (Invitrogen, USA) was used to transfer vectors into cells. PABPC1 and CHD3 siRNA were bought from RiboBio (Guangzhou, China). To constructe steady YBX1 knockdown and overexpression cell lines and organoid lines, shRNA or cDNA targeting YBX1 was cloned into pLVX-CMV-IRES-EGFP-Puro vectors (ViGene Biosciences, China). TransDux™ MAX Lentivirus Transduction Reagent (System Biosciences, CA) was used to transfer lentiviral vectors into organoids and cells. Positive cells were selected using puromycin screening 48 h following transfection. all siRNA and shRNA sequences were listed in Table S2.

2.6. Frozen section and immunofluorescence staining

After extracting organoids, we washed them with cold PBS and then digested them with a Cell Recovery solution (354253, Corning, New York). 4 % paraformaldehyde (P0099, Beyotime, China) was used to fix cell for 20 min. Organoids were dehydrated in a 30 % sucrose solution for 24 h and then embed in O.C.T. gel (4583, Thermo Fisher Scientific, MA) before being frozen at −80 °C until sectioning. Frozen slices were removed from the −80° freezer to room temperature for 1 h. Proceed with permeabilization, blocking, and antibody incubation. DAPI (C1002, Beyotime, China) was used to stain the cell nuclei after adding the corresponding primary and fluorescent-labeled secondary antibodies. Finally, we mounted the slides with neutral resin and observed them under a fluorescence microscope.

2.7. Subcutaneous xenograft model

Female BALB/c nude mice and NCG (NOD/ShiltJGpt-Prkdcem26Cd52Il2rgem26Cd22/Gpt) mice aged 4–6 weeks were obtained from the Nanjing Biomedical Research Institute of Nanjing University and housed in SPF facilities. HO8910 cells were injected subcutaneously into the right axilla of nude mice (n = 5 per group). Tumor volume was measured weekly using the formula: volume = length × widthˆ2 × 1/2. Seven days after cell injection, mice were treated according to a predetermined protocol, either with or without DDP (4 mg/kg every three days) or with SU056 (20 mg/kg every three days). After 7 rounds of treatment, the mice were sacrificed, and tumors were weighed and photographed. Tumor tissues were then fixed with 4 % paraformaldehyde or frozen for further analysis.

2.8. Oraganoid orthotopic xenograft model

Organoids were injected into the abdominal cavity of 8-week-old NCG female mice. The mice were anesthetized with 0.2 ml xylazine hydrochloride injected into the abdominal cavity, shaved, and the skin around the midline of the back, 1 cm to the right, was disinfected with iodine. The skin and peritoneum of the back of the mice were cut open to enter the abdominal cavity. The ovary was pulled out of the peritoneal cavity. A 27G needle was inserted into the fat pad to inject 5×10^6 cells/

Table 1
Clinicopathological data and organoid cultures of 20 patients with ovarian cancer.

ID	Age	FIGO Stage	Pathology	Sample Source	BRCA	IC50 (μM)	Passage Time (d)
OC#13	63	IIIC	HGSOC	laparotomy	wild	25.78	10
OC#20	58	IIIC	HGSOC	laparotomy	wild	11.07	21
OC#64	56	IVA	HGSOC	puncture biopsy	wild	34.58	14
OC#100	52	IIIC	HGSOC	laparotomy	mutant	16.21	14
OC#106	65	IIIC	HGSOC	laparotomy	mutant	14.05	5
OC#108	49	IIIC	HGSOC	laparotomy	wild	26.18	14
OC#141	62	IIIB	HGSOC	laparoscopy	wild	33.1	14
OC#152	67	IIIC	HGSOC	laparotomy	wild	9.714	7
OC#160	51	IIIC	HGSOC	laparotomy	mutant	8.379	7
OC#162	69	IIIC	HGSOC	laparotomy	wild	35.41	14
OC#164	47	IIIB	HGSOC	laparotomy	wild	31.38	14
OC#166	70	IIIC	HGSOC	laparoscopy	wild	12.56	7
OC#172	76	IVB	HGSOC	laparotomy	wild	12.41	7
OC#175	53	IIIC	HGSOC	laparotomy	wild	32.26	14
OC#176	57	IIIC	HGSOC	laparotomy	wild	30.41	10
OC#177	68	IIIC	HGSOC	laparotomy	wild	23.68	7
OC#178	64	IIIC	HGSOC	laparotomy	mutant	22.15	5
OC#179	61	IVB	HGSOC	laparotomy	wild	32.92	14
OC#185	59	IIIC	HGSOC	laparotomy	wild	27.67	10
OC#186	56	IIIC	HGSOC	laparotomy	wild	25.36	10

Note: OC indicates ovarian epithelial carcinoma; HGSOC indicates high-grade serous carcinoma.

matrix gel mixture and allowed to stand for 2 min to solidify the matrix gel. The treated tissue was returned to the peritoneal cavity, then the peritoneum and skin were sutured. After 90 days of organoid injection, DDP (4 mg/kg, once a week) or SU056 (20 mg/kg, once a week) was administered according to the established protocol. After 7 treatments, the mice were euthanized, tumors were weighed and photographed. All animal experiments were carried out in accordance with the approved plan of the Institutional Animal Care Committee of the First Affiliated Hospital of Nanjing Medical University.

2.9. RNA sequencing (RNA-seq)

Total RNA was extracted from organoids or cells. The integrity and quality of the isolated RNA were evaluated using Qubit 4. Oligo(dT) was used to enrich the total mRNA sample by removing rRNA. The Ultra™ II Directional RNA Library Prep Kit for Illumina (E7765S, NEB, MA) was used to construct the library. The library was sequenced on an Illumina HiSeq X Ten sequencing platform. RNA sequencing was performed by Novogene Biotechnology LLC. The raw sequence data was publicly available at the Genome Sequence Archive at the China National Center for Bioinformation/Beijing Institute of Genomics, Chinese Academy of Sciences (HRA004576), and can be accessed at https://ngdc.cncb.ac.cn/gsa-human [23].

2.10. RNA immunoprecipitation sequencing (RIP-seq)

The RNA immunoprecipitation (RIP) assay was performed according to the method described previously [24]. In brief, cells were lysed with lysis buffer, and the lysate was centrifuged to obtain the supernatant. The lysate was incubated with specific antibodies against the protein of interest and then subjected to immunoprecipitation using magnetic beads. RNA molecules bound to the target protein were extracted, purified using the Oligo Clean & Concentrator kit (ZYMO RESEARCH, CA), and analyzed downstream using qRT-PCR or high-throughput sequencing. High-throughput sequencing was performed by Novogene Biotechnology LLC (Novogene, Beijing). RIP specificity was validated by comparing the results with appropriate controls. All experiments were conducted under sterile conditions to avoid contamination. The raw sequence data reported in this paper had been deposited in the Genome Sequence Archive (HRA004707). Antibody information used was provided in Table S3.

2.11. Bioluminescent repair reporter (BLRR) system assay

The system-associated plasmids were purchased from Addgene (Catalog No: 158958). pLenti-BLRR was a gift from Charles P. Lai (Addgene plasmid # 158958). The protocol for this was originated from previous research [25]. Of note, 5 replicates we designed for every treatment.

2.12. Assay for Transposase-accessible chromatin (ATAC-seq)

According to the method previously described, ATAC-seq (Assay for Transposase-Accessible Chromatin using sequencing) detection was performed [26]. In simple terms, nuclei were isolated from cells and treated with Tn5 transposase (TD502, Vazyme, China) to fragment accessible regions of chromatin. The resulting fragments were then amplified by PCR, and their size distribution was evaluated by gel electrophoresis before constructing a library for high-throughput sequencing. Quality control was performed on the resulting sequencing data, and reads were aligned to a reference genome. Data analysis was then carried out to identify accessible chromatin regions, including peaks, footprints, and differences in accessibility between experimental groups. High-throughput sequencing was performed by Novogene Biotechnology LLC. All experiments were conducted under sterile conditions and appropriate controls were used to verify the specificity and sensitivity of the detection. The raw sequence data had been deposited in the Genome Sequence Archive (HRA004583).

2.13. Dot blot assay

mRNA was isolated and purified from total RNA using the mRNA Purification Kit (Beyotime). All procedures were performed according to the instructions provided with the kit. After quantification and denaturation at 95 °C for 5 min, the mRNA was loaded onto Amersham HyBond N+ membrane (Amersham, UK). The mRNA was cross-linked to the membrane twice by UV irradiation. As a control, methylene blue was incubated with mRNA and photographed. The membrane was washed with PBS containing 0.1 % Tween 20, blocked with 5 % skim milk, and then incubated overnight at 4 °C with anti-m5C antibody. The secondary antibody conjugated with horseradish peroxidase was used for detection. The antibodies used for western blotting were listed in Table S3.

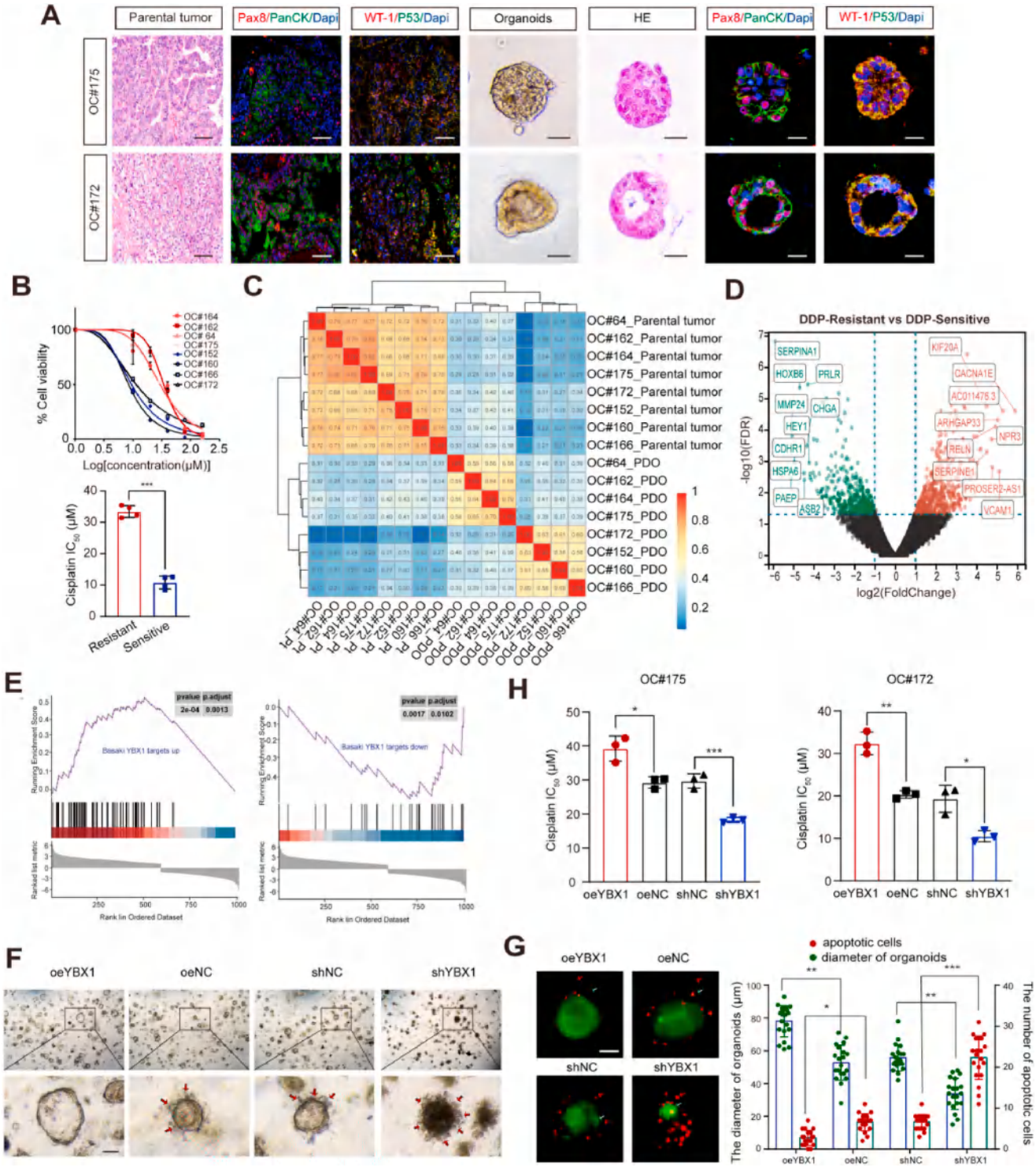

Fig. 1. High expression of YBX1 reduces sensitivity to platinum drugs in ovarian cancer organoids. (A) The pathological characteristics of DDP-resistant and DDP-sensitive organoids. The small images from left to right represent the following: an HE-stained image of the parental tissue, the expression of PAX8/PanCK in the tissues, the expression of WT-1/P53 in the tissue, a bright field image of the organoids, an HE-stained image of the organoids, the expression of PAX8/PanCK in the organoids, and the expression of WT-1/P53 in the organoids. The red fluorescence represented Pax8 and WT-1, the green fluorescence represented PanCK and P53, and the blue color represented cell nuclei. The scale represented 40 μm. (B) The IC50 curves and average IC50 values of four DDP-resistant and DDP-sensitive organoids used for RNA-seq. IC50 values was calculated by using a curve fitting model with a four-parameter logistic equation model, $***p < 0.001$. (C) Cluster analysis of differentially expressed genes between DDP-resistant or DDP-sensitive PDOs and parental tumors. (D) The volcano plot of differentially expressed genes between DDP-resistant and DDP-sensitive PDOs based on RNA-seq. (E) GSEA analysis of up- and down-regulated genes in DDP-resistant and DDP-sensitive organoids. (F) After 48 h of treatment with 30 μM cisplatin, various organoid lines exhibited changes in morphology under a light microscope. The red arrows indicated apoptotic cells. The IC50 values of each group are as follows: $IC50_{oeYBX1} = 35.23$ μM, $IC50_{oeNC} = 21.2$ μM, $IC50_{shNC} = 21.34$ μM, $IC50_{shYBX1} = 9.254$ μM. (G) SYTO 9/PI staining allowed for the simultaneous detection of live and dead cells in organoid lines. Green fluorescence represented live cells, while red fluorescence represented dead cells. (H) Statistical analysis of the IC50 values of various oganoid lines, $*p < 0.05$, $**p < 0.01$, $***p < 0.001$.

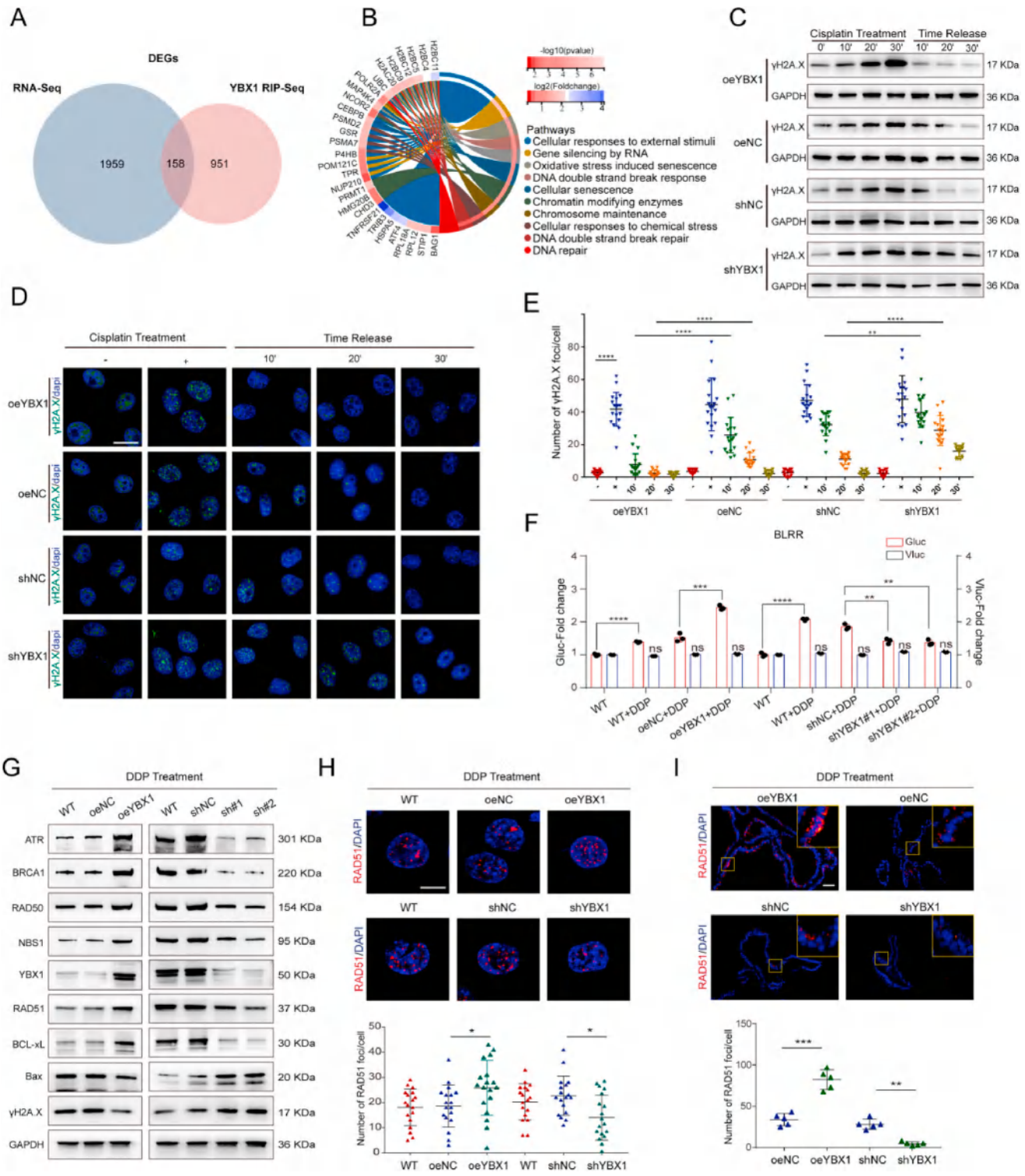

Fig. 2. YBX1 enhances tumor cell homologous recombination repair. (A) The Venn diagram of differentially expressed genes obtained from RNA sequencing (RNA-seq) and YBX1 immunoprecipitation sequencing (RIP-seq) in HO8910 cells. (B) GSEA analysis of differentially expressed genes. (C) Western blot analysis was conducted to determine the expression levels of γH2A.X in each group of HO8910 cells. (D) Representative images of γH2A.X immunofluorescent foci of HO8910 cells changed over time with cisplatin treatment. The scale bar represented 20 μm. (E) The number of γH2A.X immunofluorescence foci of HO8910 cells changed over time with cisplatin treatment. (F) The Bioluminescence Repair Reporting System (BLRR) indicated that YBX1 played an important role in homologous recombination (HR) repair rather than non-homologous end joining (NHEJ) repair. (G) The protein expression levels of HR pathway-related proteins (ATR, BRCA1, RAD50, NBS1, RAD51), apoptotic protein (Bax), anti-apoptotic protein (BCL-xL), and DNA damage marker (γH2A.X) were detected by Western blotting after YBX1 overexpression or knockdown in HO8910 cells. (H) The representative images and statistics of RAD51 foci in each experimental group of HO8910 cells were shown below. The scale bar represented 20 μm *P < 0.05, **P < 0.01, ***P < 0.001, n = 18. (I) The representative immunofluorescence images of RAD51 foci in different experimental groups of the organoids were shown, with a scale bar indicating 40 μm.

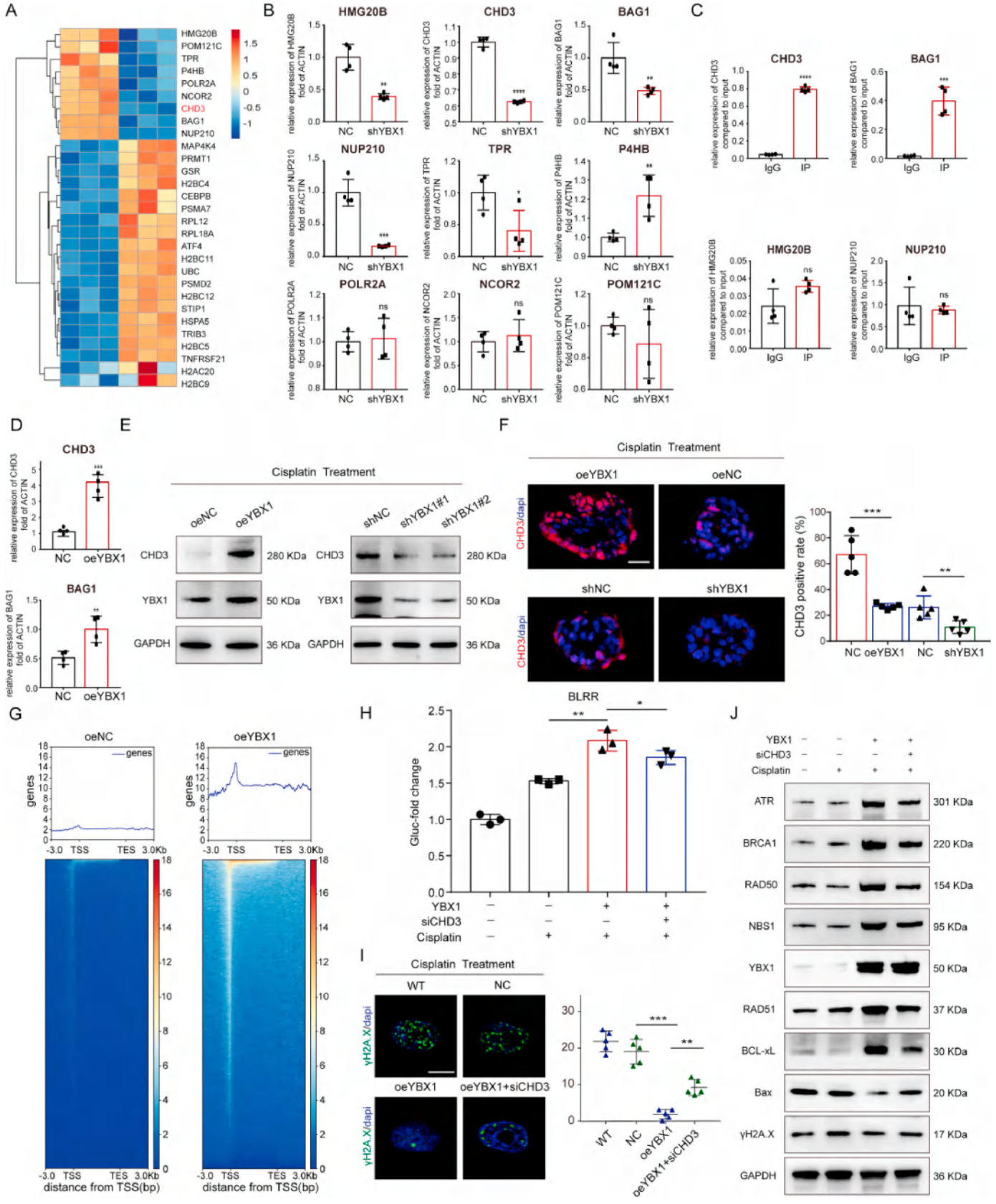

(caption on next page)

Fig. 3. YBX1 enhances chromatin accessibility by promoting CHD3 expression. (A) The heatmap of genes related to DNA damage repair overlaps between RNA-seq and RIP-seq in HO8910 cells. (B) After knocking down YBX1, the downstream genes' expressions was validated using qRT-PCR in HO8910 cells. (C) Validation of downstream genes' binding to YBX1 using RIP-PCR in HO8910 cells. (D) After the overexpression of YBX1, the expression of CHD3 and BAG1 mRNA were verified by qRT-PCR in HO8910 cells. *P < 0.05, **P < 0.01, ***P < 0.001. (E) Western blot was used to verify the expression of CHD3 protein after overexpression or knockdown of YBX1 in HO8910 cells. (F) After overexpression or knockdown of YBX1 in the organoids, the immunofluorescence image of CHD3 was shown in red, while the blue represented the cell nucleus. The scale bar indicated 40 μm. (G) ATAC-seq was employed to assess the chromatin accessibility of HO8910 cells overexpressing YBX1 under cisplatin stress. Higher peaks indicated more open chromatin and stronger accessibility. (H) After knocking down CHD3, the BLRR displayed a decrease in HR repair activity. (I) After knocking down the CHD3 gene, the number of γH2A.X immunofluorescence foci of the oeYBX1 group was rescued partly in HO8910 cells. The scale bar represents 20 μm. (J) Western blot analysis revealed that the expression level of HR pathway proteins was partly reversed upon knocking down CHD3 in HO8910 cells.

2.14. Methylated RNA immunoprecipitation sequencing (MeRIP-Seq)

According to reports, most of m5C is distributed in tRNA and rRNA. In order to minimize the influence of tRNA and rRNA, we used Dynabeads mRNA Purification Kit (ThermoFisher) to purify mRNA. The enrichment of m5C was based on the previously reported methods [16]. Briefly, 5 μg of mRNA fragments within the 100–200 nt range with IgG or m5C antibodies was incubated at 4 °C for 2 h. Protein A magnetic beads were added and incubated for another 2 h. Magnetic beads were separated using a magnet, washing 5 times with wash buffer. RNA was obtained by cutting the antibody using proteinase K enzyme. RNA was purified further using the Oligo Clean & Concentrator kit (ZYMO RESEARCH, CA) for downstream analysis such as qRT-PCR or high-throughput sequencing. High-throughput sequencing is performed by Novogene Biotechnology LLC (Novogene, Beijing). The raw sequence data had been deposited in the Genome Sequence Archive (HRA004583). The antibodies used were listed in Table S3.

2.15. Enhenced cross-linking immunoprecipitation and PCR (eCLIP-PCR)

Enhanced cross-linking immunoprecipitation was performed according to the method described previously [27]. Cells were prepared on ice and placed in a UV cross-linker to induce protein-RNA cross-linking. Cells were lysed with a lysis buffer. RNA was then fragmented with ultrasound. The supernatant was incubated with YBX1 antibody and magnetic beads was employed for capture. RNA was purified with Oligo Clean & Concentrator (ZYMO RESEARCH, CA) and analyzed with qRT-PCR. The primer sequences used for PCR were listed in Table S6.

2.16. Co-immunoprecipitation and mass spectrometry analysis

Co-Immunoprecipitation was performed using Thermo Scientific Pierce Co-IP kit. 1×10^7 cells were washed with ice-cold PBS twice, then lysed with IP lysis buffer (Beyotime). The supernatant was incubated with IgG or IP antibody at 4 °C for 2 h to form the immunoprecipitation complex. Pretreated protein A/G magnetic beads (40 μL; Invitrogen) was added to the EP tube and incubated at 4 °C for another 2 h. Target protein complex was obtained after elution buffer treated and followed by mass spectrometry analysis (Novogene, China). The antibodies used were listed in Table S3.

2.17. RNA-pulldown assay

The RNA-pulldown assay was conducted according to our previous research [28]. Briefly, 3′-biotinylated RNA probes were synthesized by Tsingke. The RNA probes were mutated to either an m5C nucleotide, an adenine nucleotide, or a guanine nucleotide. The RNA probes were transfected into cells using Lipofectamine 3000 (Invitrogen). Affinity bead (Invitrogen) were used to enrich the RNA probes and protein complexes. The protein was denatured and subjected to Western blot analysis. The RNA pulldown RNA probe sequence is shown in Table S4.

2.18. Electrophoretic mobility shift assay

1 μl of synthesized biotin-labeled RNA probes (with or without m5C, final concentration 1 mM) was mixed with purified recombinant human YBX1 protein (ab187443, Abcam, 0, 50, 100, or 200 ng) and binding buffer at room temperature for 20 min. The entire 10 μl RNA-protein mixture was produced with 1 μl of loading buffer (10 ×). The mixture was separated on a 6 % TBE gel at 80 V on ice for 45 min. The gel was transferred onto a positively charged nylon transfer membrane (GE Healthcare, IL). Chemiluminescent EMSA Kit (GS009, Beyotime, China) was employed for nucleic acid detection according to the manufacturer's instructions.

2.19. Luciferase reporter assay

A fluorescence enzyme reporting plasmid containing wild-type or mutant YBX1 3′ untranslated region (UTR) sequences was constructed by Tsingke. The plasmids were transfected into cells using Lipofectamine 3000 reagent (Invitrogen) and fluorescence enzyme detection was performed using the Dual-Luciferase Reporter Assay Kit (Promega, WI) according to the instructions. The plasmid sequences can be found in Table S5.

2.20. RNA stability assay

RNA stability was measured according to the previous description [29]. Actinomycin D (5 μg/mL; Sigma) was added to treat OC cells. Cells were harvested at specific time points. Total RNA was isolated and reversed into cDNA. PCR was used to detect intracellular RNA levels and calculate RNA degradation rate. Primer sequences were shown in Table S6.

2.21. RNA extraction and quantitative PCR

Total RNA was extracted from cells and tissues using the Animal RNA Isolation Kit (Beyotime, China), and cDNA was synthesized using the Reverse Transcription Kit (Vazyme, China) according to the manufacturer's instructions. mRNA expression was detected using the SYBR Green PCR Kit (Vazyme, China). The primer sequences used for PCR are listed in Table S6.

2.22. Western blot

The total protein of cells and tissues was lysed in RIPA buffer containing a protease inhibitor (Beyotime, China) and the protein concentration was determined by the BCA method (Beyotime, China). After protein denaturation, the expression level was detected using immunoblotting. The antibodies used were listed in Table S3.

2.23. Statistical analysis

Unpaired Student's *t*-test and One-way ANOVA were applied to examine differences between groups by GraphPad Prism 8.0.2. The IC50 values were determined using a curve fitting model with a four-parameter logistic equation model in GraphPad Prism software. Two-way ANOVA analysis was used in the statistical analysis of the subcutaneous xenograft experiment. In addition, * indicates $p < 0.05$, **indicates $p < 0.01$, *** indicates $p < 0.001$.

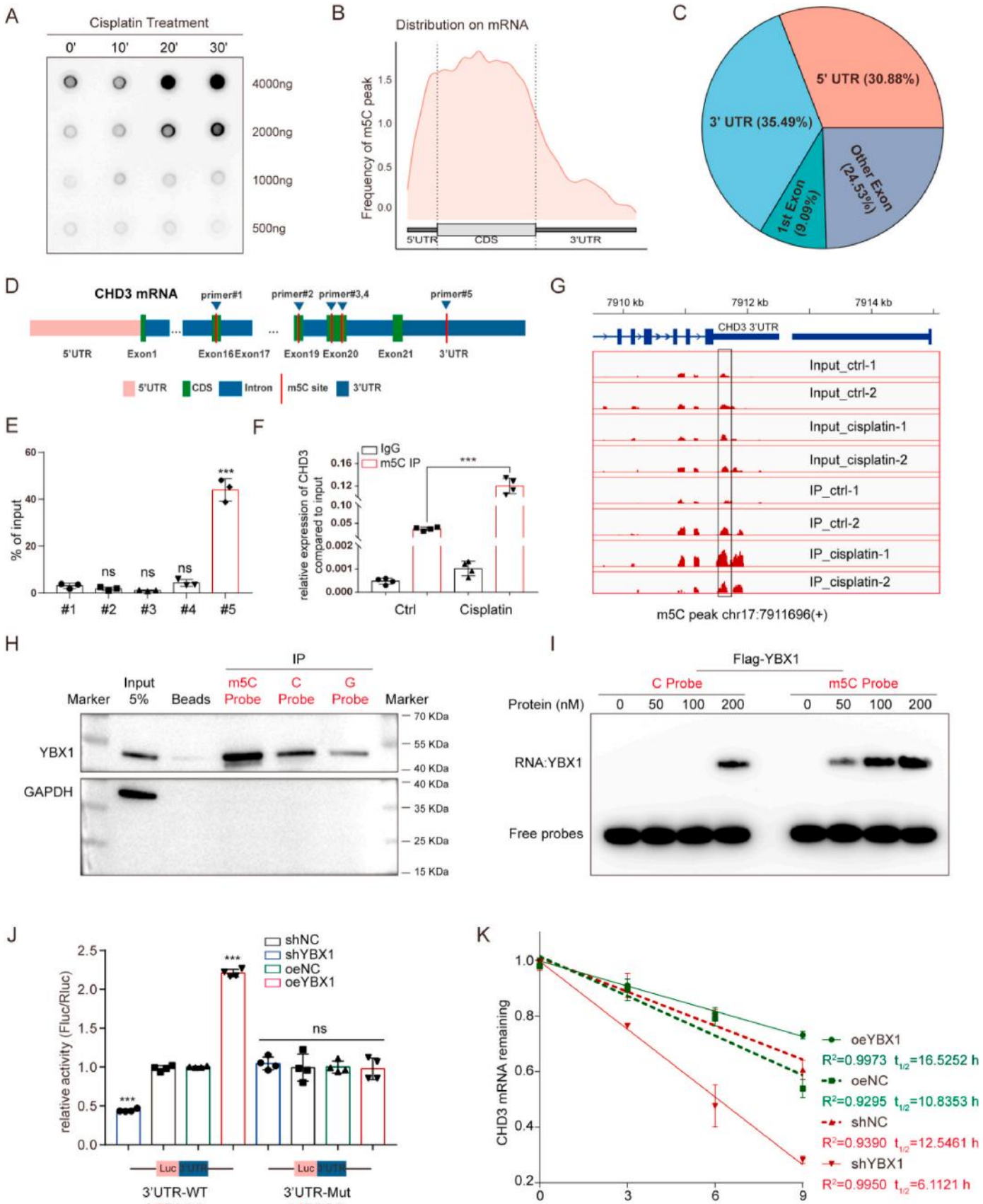

(caption on next page)

Fig. 4. YBX1 recognizes m5C modifications in CHD3 and promotes its mRNA stability. (A) The dot blot displayed the changes in the total level of m5C modification with increasing cisplatin treatment time in HO8910 cells. (B) Peak distribution of m5C modification of cells before and after cisplatin treatment in HO8910 cells. (C) Pie chart of global differential distribution of m5C modification in HO8910 cells after cisplatin treatment. (D) Diagram of m5C sites identified jointly by MeRIP sequencing and RMvar database in HO8910 cells. (E) The eCLIP-PCR confirmed that Site #5 was the binding site of YBX1 in HO8910 cells. (F) MeRIP-PCR confirmed that the m5C modification level at this site increased under cisplatin pressure in HO8910 cells. (G) IGV displayed the changes in m5C enrichment peaks among the different treatment groups at this site. (H) RNA pulldown revealed the level of YBX1 protein bound by each probe group in HO8910 cells. (I) The Electrophoretic Mobility Shift Assay (EMSA) verified the binding ability of YBX1 recombinant protein with probes containing or lacking m5C modification in HO8910 cells. (J) The dual-luciferase reporter gene system demonstrated that YBX1 bound directly to the 3′UTR region of CHD3 mRNA at position chr17:7911696 (+) and promoted expression of that transcript in HO8910 cells. (K) After treatment of cells with Actinomycin D, the half-life of CHD3 mRNA was evaluated by qRT-PCR to assess mRNA stability in HO8910 cells.

3. Results

3.1. High expression of YBX1 reduces sensitivity to platinum drugs in ovarian cancer organoids

Ovarian cancer exhibited heterogeneous phenotypes. Tumor organoids were able to preserve tumor heterogeneity and genomic stability than ex vivo cell lines. Therefore, we established ovarian cancer organoids derived from fresh tumor tissues based on the sensitivity to platinum chemotherapy. We summarized the clinical information of the patients in Table 1. These patient-derived organoids (PDOs) showed cystic or solid structures in vitro. H&E staining verified the similar structures between PDOs and primary tumor, both of which displayed extensive nuclear pleomorphism, prominent nucleoli, and dense chromatin, thereby recapitulating all features of ovarian cancer. Furthermore, they both expressed ovarian cancer markers, such as P53, Pan-CK, PAX8 & WT-1 (Fig. 1A and Supplementary Fig. 1A). Then, we calculated the IC50 of PDOs to platinum drugs and unraveled that the resistance index was negatively correlated with PFS (Supplementary Figs. 1B and C). Next, we also investigated the relationship between BRCA mutation status and IC50 values of PDOs. The results showed that the IC50 values of PDOs carrying BRCA mutations were significantly lower. However, the relationship between mutation status and PFS was not shown to be significant due to small sample size (Supplementary Fig. 1D).

We classified PDOs into platinum-sensitive and platinum-resistant groups according to their IC50 value and the PFS of patients (Fig. 1B and Supplementary Fig. 1B). RNA-seq was used to analyze the differential expression genes between the two groups. Cluster analysis demonstrated that both PDOs and parental tumor samples were able to aggregate separately and divided into DDP-resistant and DDP-sensitive groups, which indicated significant differences in gene expression profiles between the two groups (Fig. 1C). A series of chemoresistance-related genes were expressed in both PDOs and parental tumor samples, indicating genetic stability of PDOs in chemoresistance (Supplementary Fig. 1E). These results suggested that PDOs were useful tools to imitate platinum resistance of primary tumors in vitro.

To further identify the drivers of the differences in PDOs, transcriptome profiles were requested and 318 genes were analyzed to be upregulated, while 201 genes downregulated in platinum-resistant group (|log2fold change |>1, p-value <0.05) (Fig. 1E and Table S7). In order to further identify the regulatory factors of these differentially expressed genes, we performed GSEA analysis. Interestingly, the results explored that both BASAKI YBX1 targets up and BASAKI YBX1 targets down gene sets could be enriched in genes with upregulated and downregulated expression (Fig. 1F and Table S10), and YBX1 protein was highly expressed in DDP-resistant tumor samples (Supplementary Fig. 1F). This led us to speculate that YBX1 might be a critical driver in regulating platinum sensitivity in ovarian cancer.

Lentiviruses were applied to overexpress or silence YBX1 gene expression in PDOs. Indeed, the lentiviral vector exhibited high efficiency in gene expression (Supplementary Figs. 1G and H). After silencing YBX1, the organoids were collapsed when treated with cisplatin, and many scattered cell fragments were formed around the organoid (Fig. 1F), along with increased proportion of apoptotic cells (Fig. 1G and Supplementary Fig. 1I). However, no morphological changes were observed after overexpressing YBX1. Moreover, overexpressing YBX1 increased the IC50 index of DDP-sensitive PDOs. In contrast, silencing YBX1 decreased the IC50 of DDP-resistant PDOs (Fig. 1H).

3.2. YBX1 enhances homologous recombination repair of tumor cells

Although we have demonstrated that YBX1 decreased the sensitivity to the platinum drugs in ovarian cancer, the underlying mechanism is still unknown. Previous studies have suggested that YBX1 was an RNA-binding protein (RBP) that directly bound RNA and regulated RNA metabolism [30]. Therefore, we used RIP-Seq to identify YBX1-binding mRNAs. Combined with RNA-seq results, we finally obtained 158 potential genes which were regulated by YBX1 (Fig. 2A and Tables S8–9). GSEA enrichment analysis further revealed that these genes were mainly enriched in the pathways of DNA double-strand break repair, chromatin modifying enzymes and oxidative stress-induced senescence (Fig. 2B). Previous studies have suggested that platinum drugs could induce apoptosis through oxidative stress. Nevertheless, we found that YBX1 did not affect cisplatin-induced reactive oxygen in tumor cells (Supplementary Fig. 2A). From KEGG analysis of RNA-seq data, we found that the HR repair pathway was on the top rankings and many genes associated with HR were upregulated, such as POLQ, BRCA2, RAD54L, BARD1, etc (Supplementary Figs. 2B and C). As the concentrations of platinum drugs increased, both the level of DNA damage and the expression of YBX1 increased in tumor cells (Supplementary Fig. 2D). It suggested that YBX1 promoted cellular resistance to platinum drugs not by regulating oxidative stress response, but possibly by regulating DNA damage repair pathway.

To explore whether YBX1 counteracted platinum drug-induced stress by regulating the activity of DNA damage repair pathways, we established cell lines overexpressed or silencing YBX1. Cisplatin could rapidly induce DNA damage in tumor cells, forming a great many γH2A.X foci. However, after removal of cisplatin, the intracellular γH2A.X foci rapidly disappeared after overexpressing YBX1, whereas the elimination of γH2A.X foci was significantly delayed after silencing YBX1 (Fig. 2C–E). Flow cytometry confirmed that high levels of YBX1 decreased cisplatin-induced apoptosis in tumor cells, whereas silencing YBX1 increased apoptosis (Supplementary Fig. 2E). Together, this suggested that YBX1 increased the efficiency of DNA damage repair.

DSBs repair was a complex process and was mainly completed by the homologous recombination (HR) and non-homologous end joining (NHEJ) pathways. We used a bioluminescent repair reporter (BLRR) system assay to detect intracellular HR and NHEJ activities. High expression of YBX1 resulted in a significant increase in HR activity. In contrast, YBX1 knockdown suppressed HR activity. However, NHEJ activity was not affected by platinum drugs (Fig. 2F). In addition, in response to cisplatin, the expression of HR related proteins, such as BRCA1, ATR, RAD50, NBS1 and RAD51, was increased after overexpressing YBX1, but decreased after silencing YBX1 (Fig. 2G). The RAD51 protein binds to single-stranded DNA and protects the DNA from degradation during homologous recombination repair [31]. Immunofluorescence confirmed that platinum agents stimulated RAD51 foci formation in the nucleus, and in contrary, silencing YBX1 significantly reduced foci formation (Fig. 2H), which were consistent with the

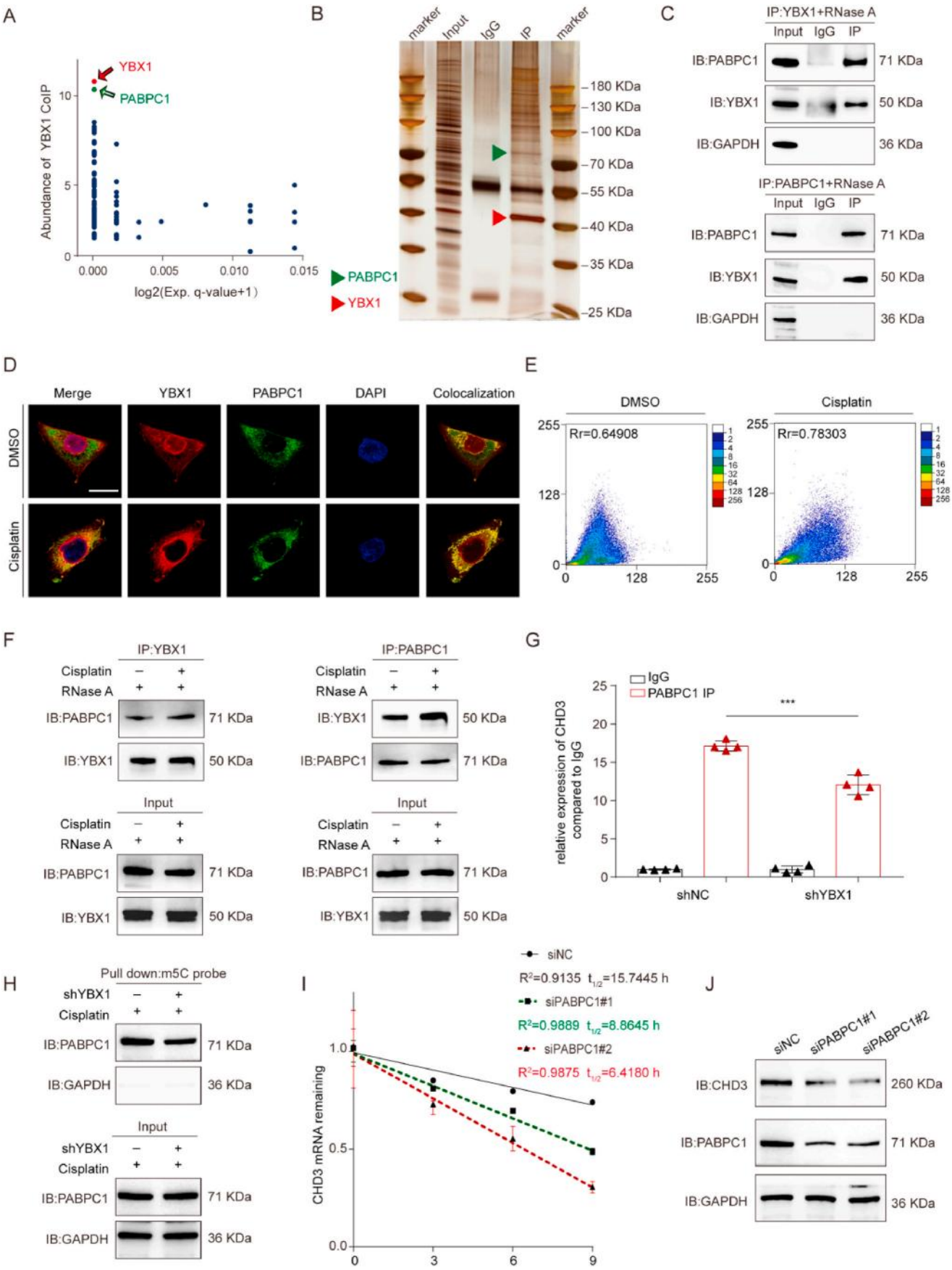

(caption on next page)

Fig. 5. PABPC1 is a critical molecular partner of YBX1 in regulating CHD3 mRNA stability. (A) The relationship between protein abundance and P-value in mass spectrometry analysis after immunoprecipitation of YBX1 in HO8910 cells. (B) Protein silver-stained image of YBX1 immunoprecipitation in HO8910 cells. (C) Western blot demonstrated the interaction between PABPC1 and YBX1 proteins in HO8910 cells. (D) Immunofluorescence indicated co-localization between YBX1 and PABPC1 under conditions with or without cisplatin in HO8910 cells. The scale bar was 20 μm. (E) Co-localization analysis of image D. (F) Western blot revealed that the binding between YBX1 and PABPC1 was enhanced in the presence of cisplatin in HO8910 cells. (G) The qRT-PCR results showed a decrease in CHD3 mRNA obtained from PABPC1 immunoprecipitation after knocking down YBX1 in HO8910 cells, with *P < 0.05, **P < 0.01, and ***P < 0.001. (H) Western blot showed a decrease in PABPC1 protein binding to the m5C probe after knocking down YBX1 in HO8910 cells. (I) After treatment with Actinomycin D, the silencing of PABPC1 decreased the half-life of CHD3 mRNA in HO8910 cells. (J) The silence of PABPC1 reduced the protein expression of CHD3 in HO8910 cells.

findings in PDOs (Fig. 2I). These indicated that YBX1 could respond to platinum drug-induced stress by regulating HR activity in tumor cells.

3.3. YBX1 enhances chromatin accessibility by promoting CHD3 expression

Although we have demonstrated that YBX1 activated the HR pathway, the precise molecular mechanism remains unclear. We figured out genes related to DNA damage repair among these 158 genes and displayed them in the heatmap (Fig. 3A). After confirming by q-PCR, of interest, only the CHD3 and BAG1 genes could response to the over-expressing or knocking down of the YBX1 gene perfectly (Fig. 3B–D). On the other hand, RIP-PCR also proved that both could bind to YBX1 protein (Fig. 3C). BAG1 protein could bind to BCL2 to exert anti-apoptotic effects, however, we found that enhancing YBX1 did not affect the expression of BAG1 protein (Supplementary Fig. 3A), indicating that BAG1 might not be a critical protein for YBX1 function.

Chromatin accessibility was prerequisite for initiating DNA damage repair. CHD3 (Chromodomain-Helicase-DNA-Binding Protein 3) was a chromatin remodeling-related enzyme that promoted DNA damage repair through enhancing chromatin remodeling [32]. We found that overexpression or knockdown of YBX1 resulted in a corresponding increase or decrease in CHD3 protein levels in HO8910 (Fig. 3E), which agreed with results in PDOs (Fig. 3F). Therefore, we assumed that YBX1 could enhance chromatin remodeling and promote DNA damage repair as response to platinum-induced stress. To verify our hypothesis, ATAC-seq was applied to assess chromatin accessibility. As expected, YBX1 was able to enhance chromatin accessibility (Fig. 3G), while silencing CHD3 by siRNA (Supplementary Fig. 3B) reduced chromatin accessibility and could partially reverse the enhancement in YBX1-overexpressed cells (Supplementary Fig. 3C). It suggested that YBX1 could potentiate chromatin accessibility by regulating CHD3 expression. In addition, through reporter gene assays, we proved that YBX1 played a role in the regulation of HR activity through CHD3. Platinum drugs would induce HR efficiency, but knockdown of CHD3 was able to compromise the function of YBX1 in promoting HR repair (Fig. 3H). This suggested that YBX1 contributed to chromatin accessibility along with HR efficiency by promoting CHD3 expression. Further, we examined the DNA damage in cells and found that silencing CHD3 resulted in higher intracellular DNA damage (Fig. 3I). Immunoblotting showed that YBX1 promoted the expression of HR-related proteins, such as BRCA1, RAD50, NBS1, RAD51, etc., but silencing CHD3 reversed the expression of these proteins (Fig. 3J).

3.4. YBX1 recognizes m5C modifications in CHD3 and promotes its mRNA stability

YBX1 was considered as an RNA binding protein (RBP) protein, and we also demonstrated that it could bind to CHD3 mRNA to regulate downstream gene expression. However, recent studies have found that YBX1 regulated mRNA metabolism in a m5C-dependent manner [33–36]. We were interested whether this novel mechanism played a role in regulating platinum drug-induced stress. In our study, the m5C modification in RNA increased rapidly after treatment of platinum drugs (Fig. 4A), suggesting that m5C modification was important in response to platinum drug stress. Then, we used MeRIP-seq to identify the distribution of m5C in mRNA, and the differential peaks of all m5C modifications were summarized in Table S11, which were mainly enriched in the 3′UTR region and CDS region (Fig. 4B and C and Supplementary Figs. 4A and B). We observed that platinum drugs induced a significant increase of m5C modification in the chr17:7911463–7912311 region of CHD3 mRNA, a region located in the 3′UTR (Fig. 4D and Table S4). To identify more conserved m5C modification loci, we queried the RMvar database, which contained all the currently reported m5C modification sites. A total of five m5C modification loci in CHD3 mRNA have been reported so far, but only one localized in the 3′UTR region (Supplementary Fig. 4C). Interestingly, this loci was also located in the region of increased m5C modification induced by platinum drugs. We designed site-specific primers for these five loci (Fig. 4E) and used eCLIP-PCR to validate the m5C modification loci induced by platinum drug stress. The YBX1 protein was identified to only bind to the sequence around the chr17:7911696 position, and the m5C modification in this region was significantly increased after platinum drug induction (Fig. 4F and G).

In contrast, we synthesized biotinylated RNA probes in vitro based on the sequence around the chr17:7911696 position. RNA-pulldown analysis revealed higher affinity of the YBX1 protein to the m5C-modified probe and was significantly reduced after mutation of this position (Fig. 4H). Electrophoretic-mobility-shift assays (EMSA) also confirmed that recombinant YBX1 protein had greater binding affinity to m5C-modified probes (Fig. 4I). This suggested that YBX1 protein not only directly recognized CHD3 mRNA, but also preferred m5C modification. To further explore the function of this binding, we used reporter gene experiments to analyze the function of the chr17:7911696 locus. As expected, knockdown or overexpression of YBX1 significantly decreased or increased luciferase activity, while no significant changes were observed after mutating this locus (Fig. 4J). RNA stability assays also confirmed that YBX1 promoted CHD3 mRNA stability (Fig. 4K). These results suggested that the YBX1 protein enhanced the stability of CHD3 mRNA through m5C binding.

3.5. PABPC1 is a critical molecular partner of YBX1 in regulating CDH3 mRNA stability

Recognition of RNA via RBP required assistance from other related proteins. To explore the proteins that synergistically regulated CHD3 mRNA stability with YBX1 protein, we performed immunoprecipitation of YBX1 protein and subjected it to mass spectrometry analysis. We found that proteins bound to YBX1 protein mainly mediated RNA binding and mRNA metabolic functions (Supplementary Figs. 5A–C). PABPC1 protein ranked first (Fig. 5A and B), which might be the cofactor of YBX1 to exert the function of RBP. Previous studies have demonstrated that PABPC1 bound to the polyA tail of mRNA to regulate the stability of RNA. To clarify whether YBX1 binding to PABPC1 protein relied on the presence of RNA, we used RNAse A to digest the RNA in the immunoprecipitation complex and further revealed that this pretreatment did not reduce the combination of these two proteins (Fig. 5C). Immunofluorescence co-localization analysis also confirmed YBX1 and PABPC1 co-localized in the cytoplasm, indicating post-transcriptional regulatory functions (Fig. 5D).

We have determined the CHD3 mRNA stability regulated by YBX1 protein was affected by platinum-induced stress. It interested us whether PABPC1 was affected. Immunofluorescence analysis confirmed a more efficient interaction between YBX1 and PABPC1 after cisplatin

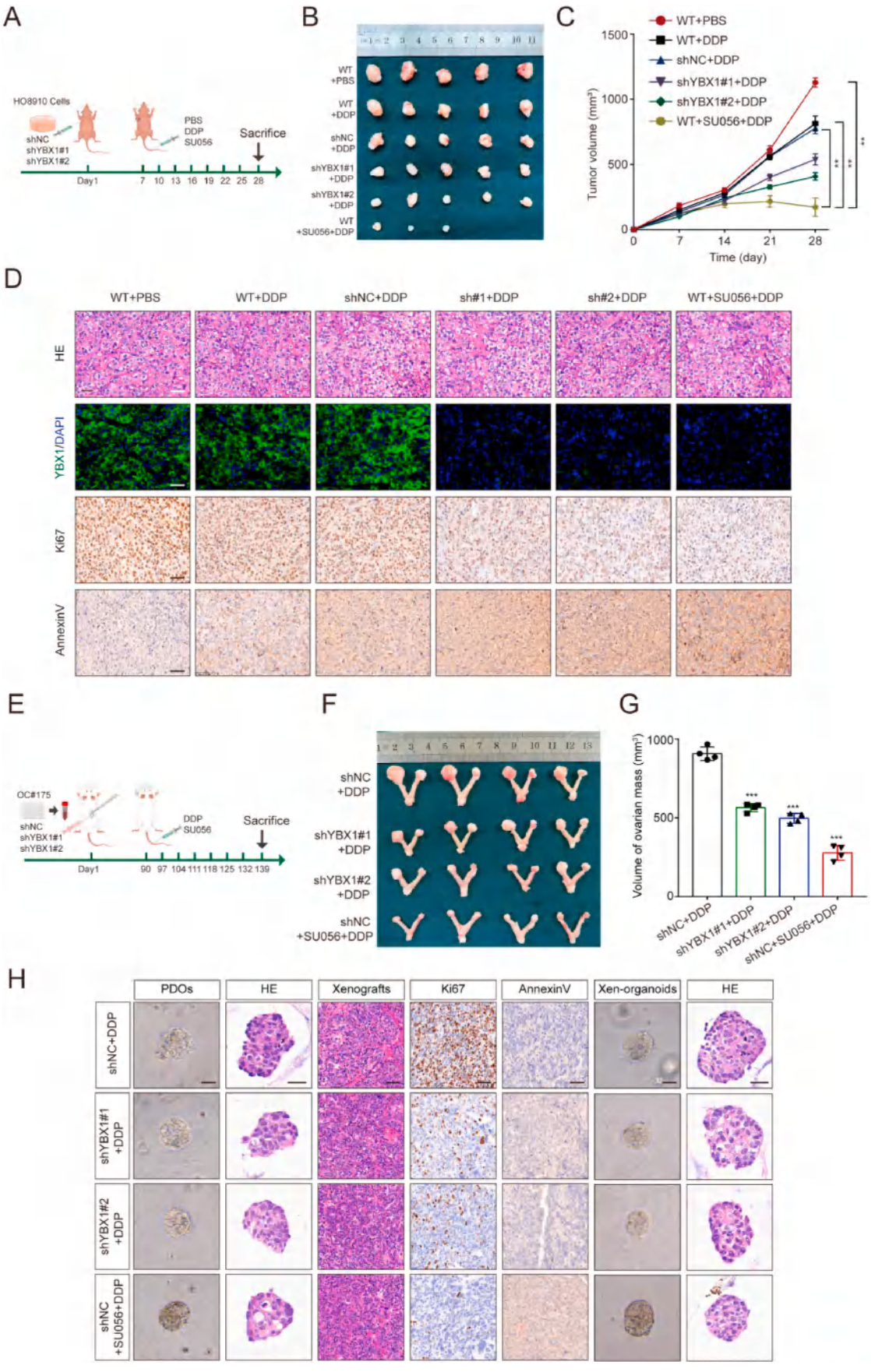

(caption on next page)

Fig. 6. YBX1 inhibition increases the sensitivity of ovarian cancer to cisplatin in vivo. (A) Diagram of establishing a subcutaneous xenograft model and administration plan. (B) Presentation of subcutaneous xenografts in each group. (C) The growth curve of subcutaneous xenograft in each group. Two-way ANOVA analysis was used in the statistical analysis of the subcutaneous xenograft experiment, $^{**}P < 0.01$, n = 5. (D) The representative images for HE staining, YBX1 immunofluorescence, Ki67 immunohistochemistry, and Annexin V immunohistochemistry of subcutaneous xenografts in each group. The scale bar was 40 μm. (E) Schematic diagram of orthotopic xenograft models establishment and administration plan. (F) Presentation of orthotopic xenografts in each group. (G) The volume of orthotopic tumors in each experimental group was analyzed, $^{*}P < 0.05$, $^{**}P < 0.01$, $^{***}P < 0.001$, n = 4. (H) The bright field images of PDOs, HE staining of PDOs, HE staining of orthotopic xenografts, Ki67 immunohistochemical staining of orthotopic xenografts, Annexin V immunohistochemical staining of orthotopic xenografts, bright field images of orthotopic xenografts organoids, HE staining of orthotopic xenografts organoids. The scale represented 40 μm.

treatment (Fig. 5D and E). Co-Immunoprecipitation analysis confirmed a tighter bonding between YBX1 and PABPC1 under cisplatin exposure (Fig. 5F). In RIP-PCR analysis, the amount of CHD3 mRNA enriched to PABPC1 protein was significantly lower in the cells silencing YBX1 than that in the wild type (Fig. 5G). Additionally, binding of PABPC1 to the m5C probe was diminished in YBX1 knockdown cells (Fig. 5H). PABPC1 was known as an important mRNA stability maintainer binding the polyA tail of the 3′UTR region of mRNA. As expected, the half-life of CHD3 mRNA was significantly shortened after silencing PABPC1 (Fig. 5I), and the protein expression of CHD3 was correspondingly reduced (Fig. 5J). These results suggested that YBX1 was an important partner for PABPC1 to stabilize mRNA.

3.6. YBX1 inhibition increases the sensitivity of ovarian cancer to cisplatin in vivo

Since we confirmed that YBX1 responded to platinum drug-induced stress, the possibility of YBX1 as a target for platinum drug resistance in the treatment of ovarian cancer raised our interest. We established a subcutaneous tumorigenic model of ovarian cancer cells and an in-situ xenograft model of PDOs. Tumor cells were injected into the axils of nude mice and dosed after 7 days according to an established protocol (Fig. 6A). SU056 was an azodiamidazole-like small molecule compound that efficiently inhibited the function of the YBX1 protein. SU056 enhanced the efficacy of paclitaxel, but its effect on the platinum drugs had not been reported. As expected, the sensitivity of tumor cells to cisplatin was increased after silencing YBX1. The combination of SU056 and cisplatin therapy resulted in a significant reduction in tumor volume compared to the group treated with cisplatin alone (Fig. 6B and C). Immunohistochemistry confirmed that inhibition of YBX1 reduced Ki-67 expression and increased expression of the apoptosis-associated protein Annexin V in tumor cells (Fig. 6D). These suggested that silencing YBX1 could inhibit tumor cell proliferation and promote tumor cell apoptosis. To better explore the pre-clinical potential of YBX1, we established orthotopic xenograft models using drug-resistant ovarian cancer organoid. Lentivirus was used to silence YBX1 expression in the organoid, which was transplanted into the peritoneal space near the ovary and inoculated for 3 months followed by drug treatment according to the established protocol (Fig. 6E). The organoid exhibited a biological behavior of invasion into the sub-peritoneal space (Supplementary Fig. 6). H&E staining confirmed that transplanted tumors exhibited extensive nuclear pleomorphism, prominent nucleoli, and dense chromatin similar to the primary tumor tissues, thereby recapitulating all features of ovarian cancer. Second-generation organoids were constructed by redigesting tissues from mouse transplant tumors, and these organoids were highly morphologically similar to patient-derived cancer organoids (Fig. 6H). It suggested that the organoid model exhibited genetic stability. After silencing YBX1, the organoid was more sensitive to cisplatin, and combined drug therapy significantly reduced tumor size (Fig. 6F and G). Furthermore, either silencing YBX1 or inhibiting YBX1 protein function resulted in lower Ki-67 expression in organoids, while expression of the apoptosis-related marker Annexin V was significantly increased. Together, this suggested that targeting YBX1 was promising to reverse platinum drug resistance (Fig. 6H).

3.7. YBX1 is highly expressed in ovarian cancer and reduces patient survival

The platinum-free interval (PFI) is defined as the time from the last day of platinum-based therapy to disease progression, which is an important predictor for the efficacy of platinum and patients' prognosis in ovarian cancer [37]. According to expert consensus, the PFI of 6 months is a common cutting-off time in ovarian cancer patients, and thus in our study, patients with a PFI <6 months were classified into platinum-resistant group, while those with a PFI ≥6 months were into platinum-sensitive group. The level of YBX1 mRNA and protein expression was significantly higher in the resistant group than that in the sensitive group (Fig. 7A and B). Immunohistochemical staining also confirmed the higher positive rate of YBX1 protein in platinum-resistant tumors (Fig. 7C and D). Since YBX1 could regulate CHD3 expression, we hypothesized that YBX1 correlated with CHD3 expression in tumors. Consistent with our hypothesis, immunohistochemical staining demonstrated that CHD3 was highly expressed in drug-resistant tumors (Fig. 7E and F and Supplementary Fig. 7A). Correlation analysis uncovered a significant positive correlation between YBX1 and CHD3 in tumor samples (Fig. 7G). Besides, according to the median level of YBX1 mRNA expression, patients with high YBX1 expression had a worse prognosis (Fig. 7H). Univariate Cox regression analysis showed that patient age, tumor stage, optimal cytoreductive surgery and YBX1 expression were significantly correlated with patient overall survival (Supplementary Fig. 7B). Multivariate Cox regression analysis confirmed that YBX1 expression was an independent predictor of patient prognosis (Supplementary Fig. 7C). Finally, we created a nomogram graph containing independent prognostic factors to predict the prognosis of ovarian cancer patients (Fig. 7I).

4. Discussion

Platinum resistance is the primary barrier affecting the prognosis of patients with ovarian cancer. Understanding how ovarian cancer cells respond to platinum-induced stress is crucial for developing therapies that can reverse platinum resistance. Y-box binding protein-1 (YBX1) has been reported to be a multifunctional oncoprotein that playing a role in cell proliferation, survival, drug resistance, and regulation of chromatin stability in tumors [20,38]. Kamura et al. found that compared to primary tumors, the expression of YBX1 was significantly increased in recurrent ovarian cancer and was associated with decreased PFS and OS in patients. The median survival period for patients with high expression of YBX1 was 25.7 months, while it was only 10.6 months for those with low expression [39]. However, Tsofack et al. found that the expression of YBX1 was not related to patients' PFS and OS [40]. The reason for their discordance may be due to the different patient populations and antibodies used in the two studies. In another study, Yahata et al. found that the abnormal high expression of nuclear YBX1 played an important role in acquired cisplatin resistance in ovarian cancer [41]. Different from the past focus on the nuclear function of YBX1, our works explained its role as an m5C reader stabilizing mRNA in the cisplatin resistant ovarian cancer, without addressing the distribution inside or outside the nucleus. In our study, we found that high levels of YBX1 expression were associated with resistance to platinum-based chemotherapy and reduced OS rates. We also discovered that YBX1 inhibition could increase the sensitivity of ovarian cancer to platinum-based

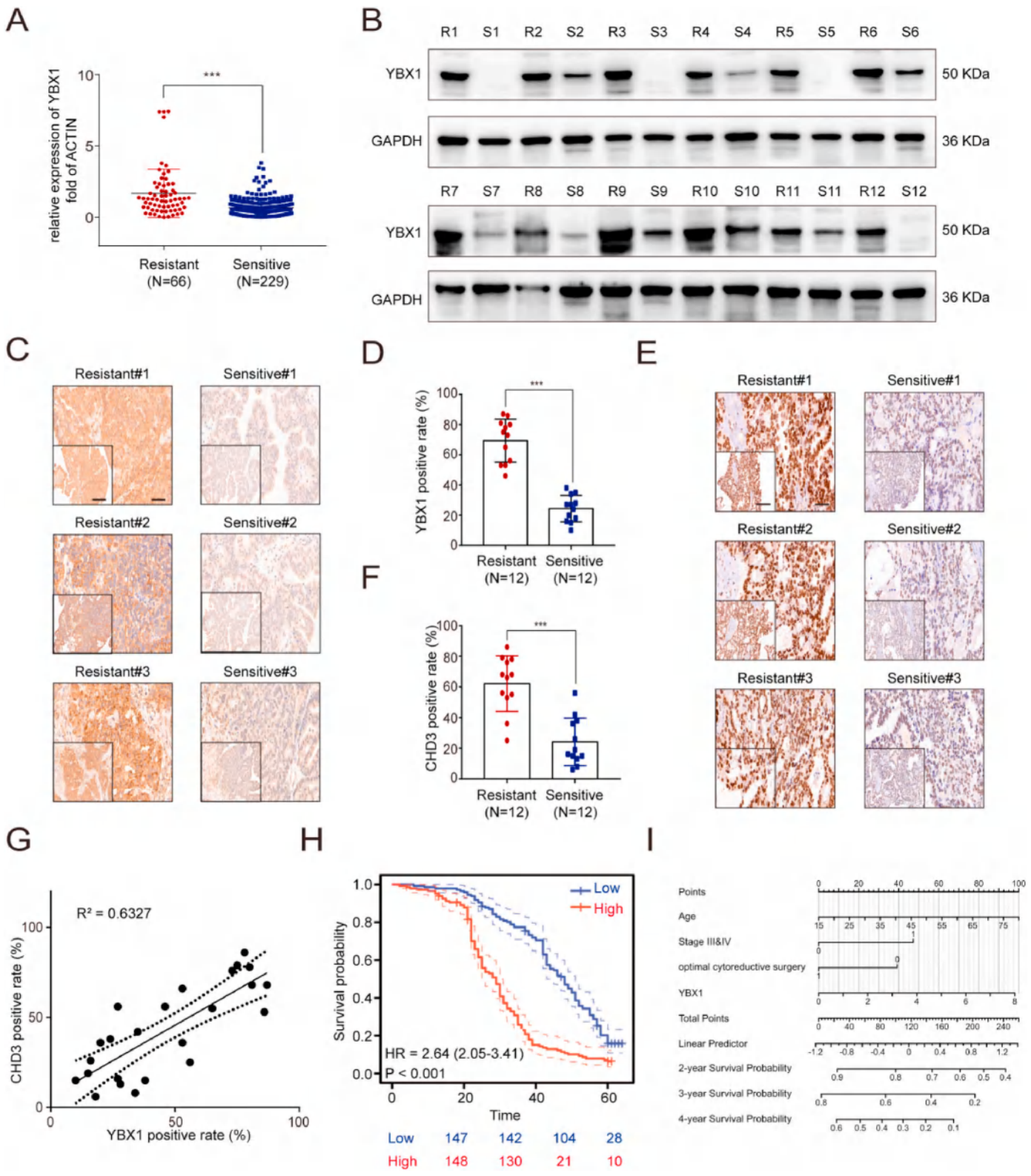

Fig. 7. YBX1 is highly expressed in ovarian cancer and reduces patient survival. (A) qRT-PCR was used to detect mRNA expression of YBX1 in DDP-resistant and DDP-sensitive ovarian cancer tissues. (B) Western blot was used to detect expression of YBX1 protein in DDP-resistant and DDP-sensitive ovarian cancer tissues. (C) Representative immunohistochemical staining of YBX1 in DDP-resistant and DDP-sensitive tissues. The scale bar was 40 μm and that at the bottom left corner was 200 μm. (D) Statistical data on YBX1 immunohistochemical staining in DDP-resistant and DDP-sensitive tissues. (E) Representative immunohistochemical staining of CHD3 in DDP-resistant and DDP-sensitive tissues. The scale bar was 40 μm and that at the bottom left corner was 200 μm. (F) Statistical data on CHD3 immunohistochemical staining in DDP-resistant and DDP-sensitive tissues. (G) The relationship between YBX1 and CHD3 immunohistochemical staining in DDP-resistant and DDP-sensitive tissues. (H) The correlation between YBX1 expression levels and overall survival (OS) among patients in our research cohort. (I) The Nomogram for predicting the prognosis of ovarian cancer, encompassing all independent prognostic factors.

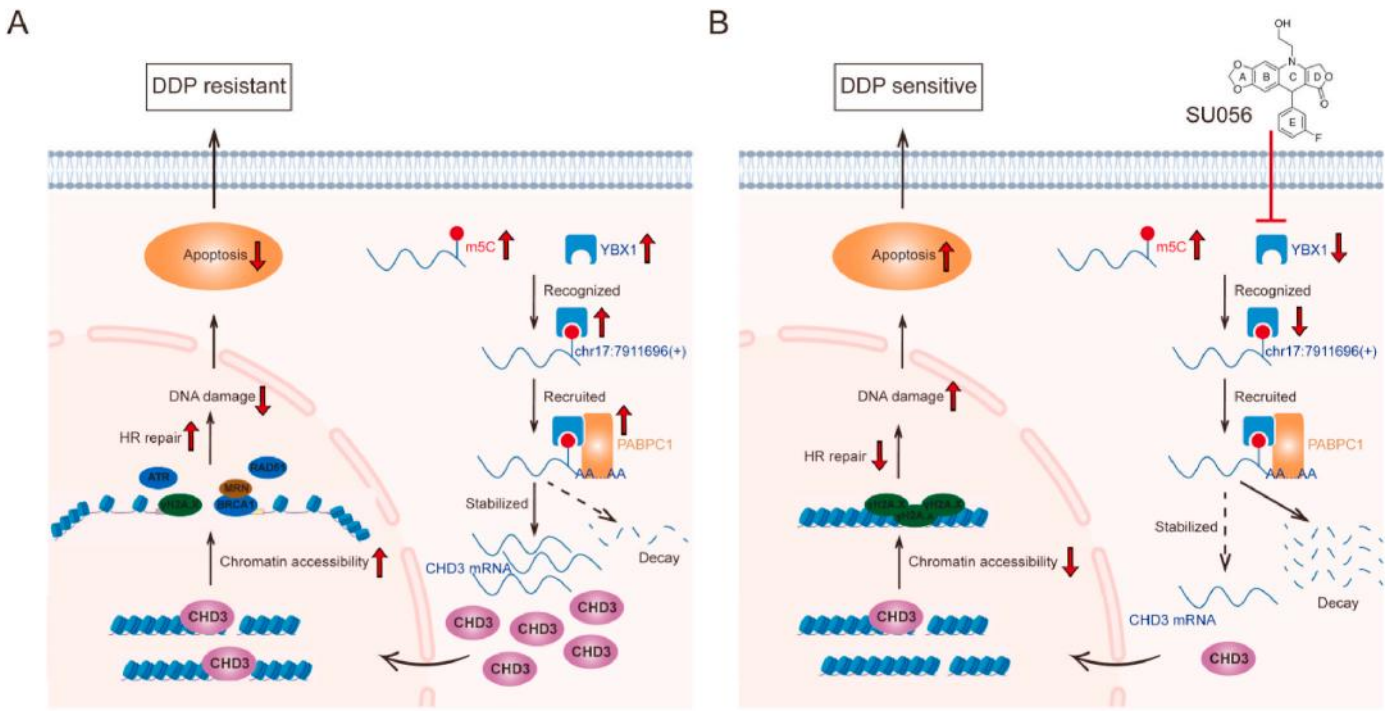

Fig. 8. The diagram of mechanism in the study.

treatments, making it a promising therapeutic target for the development of platinum-resistant therapies for ovarian cancer.

Platinum-based drugs create Pt-DNA adducts by cross-linking with DNA within cells. These adducts hinder DNA replication and transcription, prompting DNA damage repair systems to remove damaged DNA fragments and restore the DNA's integrity [42]. Therefore, an enhanced DNA damage repair capability is required to combat platinum-induced DNA damage, which is also an important mechanism for ovarian cancer cells to acquire resistance to platinum-based drugs. Previous studies have indicated that the protein YBX1 concurrently binds to DNA and regulates transcription [30]. YBX1, for instance, competes with damaged DNA sites to protect DNA from cross-linking agents, while recruiting PARP1 for DNA damage repair [43]. YBX1 promotes the transcription of various DNA repair-related genes, such as MDR1 and MVP [44]. Moreover, YBX1 binds to RNA, improving the translation of mRNA that is non-cap dependent, including Snail1, Twist, HIF1a, Lef-1, Foxo3a, and HoxC5 [30]. YBX1 also binds to some non-coding RNA, regulating their metabolism processes, such as splicing and maturation [45–47]. Nevertheless, the role of YBX1 as an RNA binding protein in DNA damage repair has not yet to be fully evaluated. This study identified that YBX1 bound to CHD3 mRNA, improving its stability and protein expression. It activated downstream homologous recombination repair pathways and promoted DNA damage repair. This might be a key mechanism for ovarian cancer cells to respond to platinum-induced stress.

CHD3 is an important member of the chromodomain helicase DNA-binding protein (CHD) family that is involved in regulating chromatin remodeling along with CHD4, MTA1, and MTA2 to form the NuRD complex [48]. It is highly expressed in malignant tumors [49,50]. The understanding of CHD3's role in chromatin remodeling regulation is currently divided. It is generally believed that CHD3 promotes the formation of heterochromatin, reduces chromatin accessibility, and suppresses DNA damage repair [51]. However, some studies have observed an increase in the level of nuclear γH2AX when CHD3 is knocked down [52]. Larsen et al. found that CHD3 is enriched at the site of double-strand breaks (DSBs) and promotes DSB repair [53]. Additionally, CHD4, another member of the NuRD complex, has been shown to recruit HR-related proteins RPA70, RAD51, and BRCA2, promoting DNA damage repair [54,55]. This may be due to the existence of different isoforms of CHD3 with different functions [52]. The results of this study showed that CHD3 was a key protein in YBX1's response to stress induced by platinum-based drugs. In detail, CHD3 expression modulated by YBX1 promoted chromatin opening and further enhanced HR repair.

The m5C modification of RNA is associated with various tumor occurrences and metastases. However, reports on the regulation of DNA damage repair by m5C modification are not well established. Li et al. discovered that mRNA containing m5C modification is situated at the DNA damage site and recruits the FMRP reader to promote transcription-coupled homologous recombination repair [56]. In this study, we observed an increase in the overall m5C modification level in ovarian cancer cells when encountered with platinum drug-induced stress, and we described the m5C modification landscape of mRNA under cisplatin stress using meRIP-seq for the first time. In recent years, YBX1 protein has been found to preferentially recognize m5C modification and regulate RNA metabolism [17,57]. Previous studies have shown that YBX1 and PABPC1 are components of stress granules (SG) that can store critical mRNA under stress conditions to protect them from degradation [58,59]. We discovered that YBX1 recognizes m5C modification in CHD3 mRNA and binds with PABPC1 protein to regulate RNA stability. We found that platinum drug-induced cellular stress enhanced the recognition and stability regulation of CHD3 mRNA by YBX1, and this regulatory mechanism depended on m5C modification. This provided clues for studying the role of m5C mechanism in stress granule formation and regulation of platinum drug resistance. Furthermore, m5C modification in RNA was dynamically regulated by "writers" or "erasers" proteins. Although we found that platinum drug-induced stress can promote overall m5C modification levels in cells, further exploration was necessary to determine the dynamically regulated mechanisms of this modification.

Cisplatin, carboplatin, and oxaliplatin are the clinical first choice for ovarian cancer treatment worldwide [60]. Carboplatin, an analog of cisplatin, exhibited anti-tumor activities and was considered as the first-line of treatment in ovarian cancer [61]. Compared with cisplatin, carboplatin exhibits a lower hydration rate [62] and has high biosafety

with greatly reduced systemic toxicity [63]. Cisplatin and carboplatin will gradually develop resistance during the treatment process. The third-generation platinum drug oxaliplatin is different from cisplatin and carboplatin, with its diaminocyclohexane ligand being hydrophobic and possessing a larger steric hindrance, which prevents the binding of repair proteins to DNA [64]. Due to its carrier group being different from other platinum drugs, the development of cross-resistance to platinum drugs is avoided. In this study, we used the classic platinum drug cisplatin as a representative to study platinum resistance in ovarian cancer, without exploring the role of YBX1 in resistance to other platinum drugs. Although the toxicity of cisplatin is relatively high, quite a few patients still use cisplatin in clinical practice. Studying the mechanism of cisplatin resistance is of great significance for overcoming the current clinical problem of platinum resistance. In future research, other platinum drugs such as carboplatin and oxaliplatin can be included.

In summary, we proposed the working model of the YBX1/m5C-CHD3/chromatin accessibility/HR repair signaling axis as an essential molecular mechanism for ovarian cancer cells to respond to platinum-induced stress. Inhibiting YBX1 significantly increased the sensitivity of ovarian cancer to platinum-induced stress (Fig. 8), highlighting the importance of targeting YBX1 to reverse platinum-resistant therapy for ovarian cancer.

CRediT authorship contribution statement

Huangyang Meng: Writing – review & editing, Writing – original draft, Visualization, Validation, Methodology, Data curation, Conceptualization. **Huixian Miao:** Writing – review & editing, Visualization, Methodology, Formal analysis. **Yashuang Zhang:** Writing – review & editing, Methodology, Formal analysis. **Tian Chen:** Writing – review & editing, Investigation, Data curation. **Lin Yuan:** Resources. **Yicong Wan:** Visualization, Funding acquisition. **Yi Jiang:** Software. **Lin Zhang:** Writing – review & editing, Validation, Methodology, Funding acquisition, Conceptualization. **Wenjun Cheng:** Writing – review & editing, Validation, Resources, Funding acquisition, Formal analysis, Conceptualization.

Declaration of competing interest

The authors declare the following financial interests/personal relationships which may be considered as potential competing interests:

Wenjun Cheng reports financial support was provided by National Natural Science Foundation of China. If there are other authors, they declare that they have no known competing financial interests or personal relationships that could have appeared to influence the work reported in this paper.

Data availability

Sequencing data have been deposited into the Genome Sequence Archive at the China National Center for Bioinformation/Beijing Institute of Genomics, Chinese Academy of Sciences and can be accessed at https://ngdc.cncb.ac.cn/gsa-human. RNA-seq data can be accessed under the SuperSeries accession number HRA004576. RIP-seq data can be accessed under the number HRA004707. ATAC-seq and meRIP-seq data can be accessed under the number HRA004583. The datasets used and/or analyzed during the current study are available from the corresponding authors on reasonable request.

Acknowledgements

This study was supported by the National Natural Science Foundation of China (No. 81872119, 82373387), National Nature Science Foundation for young scientist (No. 82103286), National Nature Science Foundation for young scientist in Jiangsu Province (No. BK20210971), Jiangsu Province 333 high level talent funds (2019), Jiangsu Province Traditional Chinese Medicine Science and Technology Development Plan Project-Key Project (No. ZD202014), General Project of Yili Clinical Medical Research Institute (2022), Jiangsu Provincial Maternal and Child Health Research Fund (2022). Jiangsu Provincial Key Medical Discipline Fund (No. ZDXK202210).

We would like to thank the Core Facility of the First Affiliated Hospital of Nanjing Medical University for its help in the experiment. We also thank "Figdraw" online tools (https://www.figdraw.com/) for some elegant model in our figure illustrations.

Appendix A. Supplementary data

Supplementary data to this article can be found online at https://doi.org/10.1016/j.canlet.2024.217064.

References

[1] R.L. Siegel, K.D. Miller, N.S. Wagle, A. Jemal, Cancer statistics, Ca-Cancer J Clin 73 (2023) 17–48, 2023.
[2] M.B. Daly, T. Pal, M.P. Berry, S.S. Buys, P. Dickson, S.M. Domchek, et al., Genetic/familial high-Risk Assessment: Breast, ovarian, and Pancreatic, Version 2.2021, NCCN clinical Practice Guidelines in Oncology, J Natl Compr Canc Ne 19 (2021) 77–102.
[3] S. Leung, P.A. Konstantinopoulos, Advances in the treatment of platinum resistant epithelial ovarian cancer: an update on standard and experimental therapies, Expert Opin Inv Drug 30 (2021) 695–707.
[4] S. Lheureux, C. Gourley, I. Vergote, A.M. Oza, Epithelial ovarian cancer, Lancet 393 (2019) 1240–1253.
[5] X. Wang, Y. Wang, S. Gou, F. Chen, A trifunctional Pt(II) complex alleviates the NHEJ/HR-related DSBs repairs to evade cisplatin-resistance in NSCLC, Bioorg. Chem. 104 (2020) 104210.
[6] S. Britton, P. Chanut, C. Delteil, N. Barboule, P. Frit, P. Calsou, ATM antagonizes NHEJ proteins assembly and DNA-ends synapsis at single-ended DNA double strand breaks, Nucleic Acids Res. 48 (2020) 9710–9723.
[7] A. Andrades, P. Peinado, J.C. Alvarez-Perez, J. Sanjuan-Hidalgo, D.J. Garcia, A. M. Arenas, et al., SWI/SNF complexes in hematological malignancies: biological implications and therapeutic opportunities, Mol. Cancer 22 (2023) 39.
[8] Z. Zhang, C. Zhou, X. Li, S.D. Barnes, S. Deng, E. Hoover, et al., Loss of CHD1 promotes heterogeneous mechanisms of resistance to AR-Targeted therapy via chromatin Dysregulation, Cancer Cell 37 (2020) 584–598.e11.
[9] A.B. Iniguez, G. Alexe, E.J. Wang, G. Roti, S. Patel, L. Chen, et al., Resistance to epigenetic-Targeted therapy Engenders tumor cell Vulnerabilities associated with enhancer remodeling, Cancer Cell 34 (2018) 922–938.e7.
[10] P. Verma, Y. Zhou, Z. Cao, P.V. Deraska, M. Deb, E. Arai, et al., ALC1 links chromatin accessibility to PARP inhibitor response in homologous recombination-deficient cells, Nat. Cell Biol. 23 (2021) 160–171.
[11] B.B. Liau, C. Sievers, L.K. Donohue, S.M. Gillespie, W.A. Flavahan, T.E. Miller, et al., Adaptive chromatin remodeling Drives glioblastoma Stem cell Plasticity and drug Tolerance, Cell Stem Cell 20 (2017) 233–246.e7.
[12] J.X. Cheng, L. Chen, Y. Li, A. Cloe, M. Yue, J. Wei, et al., RNA cytosine methylation and methyltransferases mediate chromatin organization and 5-azacytidine response and resistance in leukaemia, Nat. Commun. 9 (2018) 1163.
[13] H. Chen, H. Yang, X. Zhu, T. Yadav, J. Ouyang, S.S. Truesdell, et al., m(5)C modification of mRNA serves a DNA damage code to promote homologous recombination, Nat. Commun. 11 (2020) 2834.
[14] V.Y. Vare, E.R. Eruysal, A. Narendran, K.L. Sarachan, P.F. Agris, Chemical and Conformational Diversity of modified Nucleosides affects tRNA structure and function, Biomolecules 7 (2017).
[15] Y.S. Chen, W.L. Yang, Y.L. Zhao, Y.G. Yang, Dynamic transcriptomic m(5) C and its regulatory role in RNA processing, Wires Rna 12 (2021) e1639.
[16] X. Yang, Y. Yang, B.F. Sun, Y.S. Chen, J.W. Xu, W.Y. Lai, et al., 5-methylcytosine promotes mRNA export - NSUN2 as the methyltransferase and ALYREF as an m(5)C reader, Cell Res. 27 (2017) 606–625.
[17] X. Chen, A. Li, B.F. Sun, Y. Yang, Y.N. Han, X. Yuan, et al., 5-methylcytosine promotes pathogenesis of bladder cancer through stabilizing mRNAs, Nat. Cell Biol. 21 (2019) 978–990.
[18] L. Yang, V. Perrera, E. Saplaoura, F. Apelt, M. Bahin, A. Kramdi, et al., m(5)C methylation Guides systemic transport of Messenger RNA over Graft Junctions in Plants, Curr. Biol. 29 (2019) 2465–2476.e5.
[19] X. Niu, L. Peng, W. Liu, C. Miao, X. Chen, J. Chu, et al., A cis-eQTL in NSUN2 promotes esophageal squamous-cell carcinoma progression and radiochemotherapy resistance by mRNA-m(5)C methylation, Signal Transduct Tar 7 (2022) 267.
[20] P.K. Maurya, A. Mishra, B.S. Yadav, S. Singh, P. Kumar, A. Chaudhary, et al., Role of Y Box Protein-1 in cancer: as potential biomarker and novel therapeutic target, J. Cancer 8 (2017) 1900–1907.
[21] D.N. Lyabin, I.A. Eliseeva, L.P. Ovchinnikov, YB-1 protein: functions and regulation, Wires Rna 5 (2014) 95–110.
[22] O. Kopper, C.J. de Witte, K. Lohmussaar, J.E. Valle-Inclan, N. Hami, L. Kester, et al., An organoid platform for ovarian cancer captures intra- and interpatient heterogeneity, Nat Med 25 (2019) 838–849.

[23] T. Chen, X. Chen, S. Zhang, J. Zhu, B. Tang, A. Wang, et al., The Genome sequence Archive family: toward Explosive data growth and Diverse data types, Genom Proteom Bioinf 19 (2021) 578–583.
[24] R. Sun, L. Yuan, Y. Jiang, Y. Wan, X. Ma, J. Yang, et al., ALKBH5 activates FAK signaling through m6A demethylation in ITGB1 mRNA and enhances tumor-associated lymphangiogenesis and lymph node metastasis in ovarian cancer, Theranostics 13 (2023) 833–848.
[25] J.C. Chien, C.E. Badr, C.P. Lai, Multiplexed bioluminescence-mediated tracking of DNA double-strand break repairs in vitro and in vivo, Nat. Protoc. 16 (2021) 3933–3953.
[26] J.D. Buenrostro, B. Wu, H.Y. Chang, W.J. Greenleaf, ATAC-seq: a method for assaying chromatin accessibility Genome-wide, Curr. Protoc. Mol. Biol. 109 (2015) 21.29.1–21.29.9.
[27] E.L. Van Nostrand, G.A. Pratt, A.A. Shishkin, C. Gelboin-Burkhart, M.Y. Fang, B. Sundararaman, et al., Robust transcriptome-wide discovery of RNA-binding protein binding sites with enhanced CLIP (eCLIP), Nat. Methods 13 (2016) 508–514.
[28] C. Chen, H. Zheng, Y. Luo, Y. Kong, M. An, Y. Li, et al., SUMOylation promotes extracellular vesicle-mediated transmission of lncRNA ELNAT1 and lymph node metastasis in bladder cancer, J. Clin. Invest. 131 (2021).
[29] H. Huang, H. Weng, W. Sun, X. Qin, H. Shi, H. Wu, et al., Recognition of RNA N(6)-methyladenosine by IGF2BP proteins enhances mRNA stability and translation, Nat. Cell Biol. 20 (2018) 285–295.
[30] A. Alkrekshi, W. Wang, P.S. Rana, V. Markovic, K. Sossey-Alaoui, A comprehensive review of the functions of YB-1 in cancer stemness, metastasis and drug resistance, Cell. Signal. 85 (2021) 110073.
[31] R. Anand, E. Buechelmaier, O. Belan, M. Newton, A. Vancevska, A. Kaczmarczyk, et al., HELQ is a dual-function DSB repair enzyme modulated by RPA and RAD51, Nature 601 (2022) 268–273.
[32] R. Smith, H. Sellou, C. Chapuis, S. Huet, G. Timinszky, CHD3 and CHD4 recruitment and chromatin remodeling activity at DNA breaks is promoted by early poly(ADP-ribose)-dependent chromatin relaxation, Nucleic Acids Res. 46 (2018) 6087–6098.
[33] Y. Wang, J. Wei, L. Feng, O. Li, L. Huang, S. Zhou, et al., Aberrant m5C hypermethylation mediates intrinsic resistance to gefitinib through NSUN2/YBX1/QSOX1 axis in EGFR-mutant non-small-cell lung cancer, Mol. Cancer 22 (2023) 81.
[34] K. Liu, P. Xu, J. Lv, H. Ge, Z. Yan, S. Huang, et al., Peritoneal high-fat environment promotes peritoneal metastasis of gastric cancer cells through activation of NSUN2-mediated ORAI2 m5C modification, Oncogene 42 (2023) 1980–1993.
[35] Q. Zhang, F. Liu, W. Chen, H. Miao, H. Liang, Z. Liao, et al., The role of RNA m(5)C modification in cancer metastasis, Int. J. Biol. Sci. 17 (2021) 3369–3380.
[36] Y. Chen, X. Zuo, Q. Wei, J. Xu, X. Liu, S. Liu, et al., Upregulation of LRRC8A by m(5)C modification-mediated mRNA stability suppresses apoptosis and facilitates tumorigenesis in cervical cancer, Int. J. Biol. Sci. 19 (2023) 691–704.
[37] L.J. St, J.F. Liu, Treatment Approaches for platinum-resistant ovarian cancer, J. Clin. Oncol. 42 (2024) 127–133.
[38] T. Ohga, K. Koike, M. Ono, Y. Makino, Y. Itagaki, M. Tanimoto, et al., Role of the human Y box-binding protein YB-1 in cellular sensitivity to the DNA-damaging agents cisplatin, mitomycin C, and ultraviolet light, Cancer Res. 56 (1996) 4224–4228.
[39] T. Kamura, H. Yahata, S. Amada, S. Ogawa, T. Sonoda, H. Kobayashi, et al., Is nuclear expression of Y box-binding protein-1 a new prognostic factor in ovarian serous adenocarcinoma? Cancer-Am Cancer Soc 85 (1999) 2450–2454.
[40] A. Siraj, V. Desestret, M. Antoine, G. Fromont, M. Huerre, M. Sanson, et al., Expression of follicle-stimulating hormone receptor by the vascular endothelium in tumor metastases, BMC Cancer 13 (2013) 246.
[41] H. Yahata, H. Kobayashi, T. Kamura, S. Amada, T. Hirakawa, K. Kohno, et al., Increased nuclear localization of transcription factor YB-1 in acquired cisplatin-resistant ovarian cancer, J Cancer Res Clin 128 (2002) 621–626.
[42] G. Speelmans, R.W. Staffhorst, K. Versluis, J. Reedijk, B. de Kruijff, Cisplatin complexes with phosphatidylserine in membranes, Biochemistry-Us 36 (1997) 10545–10550.
[43] E.E. Alemasova, P.E. Pestryakov, M.V. Sukhanova, D.A. Kretov, N.A. Moor, P. A. Curmi, et al., Poly(ADP-ribosyl)ation as a new posttranslational modification of YB-1, Biochimie 119 (2015) 36–44.
[44] T. Tanaka, H. Saito, S. Miyairi, S. Kobayashi, 7-Hydorxyindirubin is capable of specifically inhibiting anticancer drug-induced YB-1 nuclear translocation without showing cytotoxicity in HepG2 hepatocellular carcinoma cells, Biochem Bioph Res Co 544 (2021) 15–21.
[45] X. Wang, X. Zhang, Y. Dang, D. Li, G. Lu, W.Y. Chan, et al., Long noncoding RNA HCP5 participates in premature ovarian insufficiency by transcriptionally regulating MSH5 and DNA damage repair via YB1, Nucleic Acids Res. 48 (2020) 4480–4491.
[46] S.L. Wu, X. Fu, J. Huang, T.T. Jia, F.Y. Zong, S.R. Mu, et al., Genome-wide analysis of YB-1-RNA interactions reveals a novel role of YB-1 in miRNA processing in glioblastoma multiforme, Nucleic Acids Res. 43 (2015) 8516–8528.
[47] G. Grigelioniene, H.I. Suzuki, F. Taylan, F. Mirzamohammadi, Z.U. Borochowitz, U. M. Ayturk, et al., Gain-of-function mutation of microRNA-140 in human skeletal dysplasia, Nat Med 25 (2019) 583–590.
[48] H. Hoffmeister, A. Fuchs, F. Erdel, S. Pinz, R. Grobner-Ferreira, A. Bruckmann, et al., CHD3 and CHD4 form distinct NuRD complexes with different yet overlapping functionality, Nucleic Acids Res. 45 (2017) 10534–10554.
[49] C.G. Marfella, A.N. Imbalzano, The Chd family of chromatin remodelers, Mutat Res-Fund Mol M 618 (2007) 30–40.
[50] H.P. Seelig, M. Renz, I.N. Targoff, Q. Ge, M.B. Frank, Two forms of the major antigenic protein of the dermatomyositis-specific Mi-2 autoantigen, Arthritis Rheum. 39 (1996) 1769–1771.
[51] A.A. Goodarzi, T. Kurka, P.A. Jeggo, KAP-1 phosphorylation regulates CHD3 nucleosome remodeling during the DNA double-strand break response, Nat. Struct. Mol. Biol. 18 (2011) 831–839.
[52] H. Brunton, A.A. Goodarzi, A.T. Noon, A. Shrikhande, R.S. Hansen, P.A. Jeggo, et al., Analysis of human syndromes with disordered chromatin reveals the impact of heterochromatin on the efficacy of ATM-dependent G2/M checkpoint arrest, Mol. Cell Biol. 31 (2011) 4022–4035.
[53] D.H. Larsen, C. Poinsignon, T. Gudjonsson, C. Dinant, M.R. Payne, F.J. Hari, et al., The chromatin-remodeling factor CHD4 coordinates signaling and repair after DNA damage, J. Cell Biol. 190 (2010) 731–740.
[54] M.R. Pan, H.J. Hsieh, H. Dai, W.C. Hung, K. Li, G. Peng, et al., Chromodomain helicase DNA-binding protein 4 (CHD4) regulates homologous recombination DNA repair, and its deficiency sensitizes cells to poly(ADP-ribose) polymerase (PARP) inhibitor treatment, J. Biol. Chem. 287 (2012) 6764–6772.
[55] S.E. Polo, A. Kaidi, L. Baskcomb, Y. Galanty, S.P. Jackson, Regulation of DNA-damage responses and cell-cycle progression by the chromatin remodelling factor CHD4, Embo J 29 (2010) 3130–3139.
[56] H. Yang, Y. Wang, Y. Xiang, T. Yadav, J. Ouyang, L. Phoon, et al., FMRP promotes transcription-coupled homologous recombination via facilitating TET1-mediated m5C RNA modification demethylation, P Natl Acad Sci Usa 119 (2022) e2116251119.
[57] Y. Chen, X. Zuo, Q. Wei, J. Xu, X. Liu, S. Liu, et al., Upregulation of LRRC8A by m(5)C modification-mediated mRNA stability suppresses apoptosis and facilitates tumorigenesis in cervical cancer, Int. J. Biol. Sci. 19 (2023) 691–704.
[58] K. Budkina, H.K. El, M.J. Clement, B. Desforges, A. Bouhss, V. Joshi, et al., YB-1 unwinds mRNA secondary structures in vitro and negatively regulates stress granule assembly in HeLa cells, Nucleic Acids Res. 49 (2021) 10061–10081.
[59] J.M. Burke, S.L. Moon, T. Matheny, R. Parker, RNase L Reprograms translation by Widespread mRNA Turnover Escaped by Antiviral mRNAs, Mol Cell 75 (2019) 1203–1217.e5.
[60] C. Zhang, C. Xu, X. Gao, Q. Yao, Platinum-based drugs for cancer therapy and anti-tumor strategies, Theranostics 12 (2022) 2115–2132.
[61] S. Tendulkar, S. Dodamani, Chemoresistance in ovarian cancer: Prospects for new drugs, Anti-Cancer Agent Me 21 (2021) 668–678.
[62] S. Dilruba, G.V. Kalayda, Platinum-based drugs: past, present and future, Cancer Chemoth Pharm 77 (2016) 1103–1124.
[63] G.Y. Ho, N. Woodward, J.I. Coward, Cisplatin versus carboplatin: comparative review of therapeutic management in solid malignancies, Crit Rev Oncol Hemat 102 (2016) 37–46.
[64] R.J. Browning, P. Reardon, M. Parhizkar, R.B. Pedley, M. Edirisinghe, J. C. Knowles, et al., Drug Delivery strategies for platinum-based chemotherapy, ACS Nano 11 (2017) 8560–8578.